

# Long-Term Monitoring of Utility-Scale Solar Energy Development and Application of Remote Sensing Technologies: Summary Report

---

Environmental Science Division



### **About Argonne National Laboratory**

Argonne is a U.S. Department of Energy laboratory managed by UChicago Argonne, LLC under contract DE-AC02-06CH11357. The Laboratory's main facility is outside Chicago, at 9700 South Cass Avenue, Argonne, Illinois 60439. For information about Argonne and its pioneering science and technology programs, see [www.anl.gov](http://www.anl.gov).

### **DOCUMENT AVAILABILITY**

**Online Access:** U.S. Department of Energy (DOE) reports produced after 1991 and a growing number of pre-1991 documents are available free via DOE's SciTech Connect (<http://www.osti.gov/scitech/>).

### **Reports not in digital format may be purchased by the public from the National Technical Information Service (NTIS):**

U.S. Department of Commerce  
National Technical Information Service  
5301 Shawnee Rd  
Alexandria, VA 22312  
**[www.ntis.gov](http://www.ntis.gov)**  
Phone: (800) 553-NTIS (6847) or (703) 605-6000  
Fax: (703) 605-6900  
Email: [orders@ntis.gov](mailto:orders@ntis.gov)

### **Reports not in digital format are available to DOE and DOE contractors from the Office of Scientific and Technical Information (OSTI):**

U.S. Department of Energy  
Office of Scientific and Technical Information  
P.O. Box 62  
Oak Ridge, TN 37831-0062  
**[www.osti.gov](http://www.osti.gov)**  
Phone: (865) 576-8401  
Fax: (865) 576-5728  
Email: [reports@osti.gov](mailto:reports@osti.gov)

### **Disclaimer**

This report was prepared as an account of work sponsored by an agency of the United States Government. Neither the United States Government nor any agency thereof, nor UChicago Argonne, LLC, nor any of their employees or officers, makes any warranty, express or implied, or assumes any legal liability or responsibility for the accuracy, completeness, or usefulness of any information, apparatus, product, or process disclosed, or represents that its use would not infringe privately owned rights. Reference herein to any specific commercial product, process, or service by trade name, trademark, manufacturer, or otherwise, does not necessarily constitute or imply its endorsement, recommendation, or favoring by the United States Government or any agency thereof. The views and opinions of document authors expressed herein do not necessarily state or reflect those of the United States Government or any agency thereof, Argonne National Laboratory, or UChicago Argonne, LLC.

# **Long-Term Monitoring of Utility-Scale Solar Energy Development and Application of Remote Sensing Technologies: Summary Report**

---

prepared by  
Yuki Hamada, Mark A. Grippo, and Karen P. Smith  
Environmental Science Division, Argonne National Laboratory

September 2014



# CONTENTS

NOTATION.....	vii
EXECUTIVE SUMMARY .....	1
1 INTRODUCTION.....	5
2 STUDY AREA .....	9
3 METHODOLOGY OVERVIEW .....	11
3.1 Data.....	11
3.2 Data Processing.....	14
3.2.1 Extraction of Surface Hydrological Features.....	14
3.2.2 Vegetation Characterization .....	18
3.2.2.1 Characterization of Vegetation Distribution and Fractional Cover of Surface Types.....	18
3.2.2.2 Estimation of Vegetation Height.....	20
3.2.3 Surface Stability and Soil Properties .....	22
3.2.3.1 A New Remote Sensing Metric for Assessing Soil and Site Stability, the Erosion Resistance Index.....	22
3.2.3.2 Soil Properties and Remote Sensing Metrics .....	23
3.2.3.3 Biological Soil Crust and Remote Sensing Metric, the Biological Soil Crust Index .....	24
4 RESULTS AND SYNTHESIS.....	27
4.1 Surface Hydrologic Features.....	27
4.2 Characterization of Vegetation and Vegetated Surface .....	30
4.2.1 Vegetation Distribution and Fractional Cover of Surface Types .....	30
4.2.2 Vegetation Height Estimate.....	35
4.3 Soil and Surface Properties.....	37
4.3.1 A New Remote Sensing Metric for Assessing Surface Stability, the Erosion Resistance Index.....	37
4.3.2 Soil Properties and Remote Sensing Metrics.....	39
4.3.3 Biological Soil Crust and Remote Sensing Metrics.....	40
4.4 Effective Remote Sensing Metrics for Extracting and Characterizing Desert Landscape Features and Properties.....	41
5 CONCLUSIONS AND FUTURE WORK.....	45
6 REFERENCES .....	49

## FIGURES

1	Study Area .....	9
2	Workflow Overview of Ephemeral Stream Channel Extraction Using Very High Spatial Resolution Multispectral Image.....	17
3	Workflow Overview of Vegetation Distribution and Cover Estimation Using the Very High Spatial Resolution Multispectral Image.....	19
4	Workflow Overview of Vegetation Height Estimation Using the Very High Spatial Resolution Multispectral Image.....	21
5	Scatter Plot of a Green/Red Band-Ratio versus a Red/NIR Band-Ratio by Surface Type for Correspondence to a Range of Erosion Risks.....	23
6	Maps of Ephemeral Stream Channels Derived from the Very High Spatial Resolution Image .....	28
7	Close-Up Views of Vegetation Distribution Maps Derived from the Very High Spatial Resolution Image .....	31
8	Close-Up Views of Fractional Cover Maps of Surface Types Derived from the Very High Spatial Resolution Image .....	33
9	Correlation between Reference Cover and Cover Estimated Using Remote Sensing, Calculated Using All Plots and Excluding Plot 7 .....	35
10	Correlation between Recorded Vegetation Height and Plant Height Estimated Using Remote Sensing and Modeled Vegetation Height with Accuracy Measures.....	36
11	Close-Up Views of Very High Spatial Resolution Image Feature-Based Vegetation Height Map Derived from Image-Based Point-Cloud Data.....	37
12	Close-Up View of Surface Stability Index Maps Derived from the Very High Spatial Resolution Image .....	38
13	Close-Up Views of Biological Soil Crust Index Maps Derived from the Very High Spatial Resolution Image.....	42

## TABLES

1	Summary of Remotely Sensed Data .....	12
2	Summary of Field Survey and Sample Data.....	13
3	Monitoring Indicators and Relevant Remote Sensing Metrics Considered.....	15
4	Accuracy of Ephemeral Stream Channel Maps Derived from Remotely Sensed Imagery .....	29
5	Accuracy of Vegetation Distribution Map Derived from Remotely Sensed Imagery .....	32
6	Accuracy of Surface Type Fractional Cover Maps Derived from Remotely Sensed Imagery .....	34
7	Pairwise t-Test Results for the Comparison of the Erosion Resistance Index Values for Five Land Surface Cover Types.....	39
8	Correlation Analysis Results for the Relationships between Remote Sensing Metrics and Soil Properties.....	40
9	Equations Describing the Relationship of Remote Sensing Metrics to Soil Properties .....	41
10	Monitoring Indicators Tested and Remote Sensing Metrics Identified in This Study .....	42

*This page intentionally left blank.*

## NOTATION

The following is a list of acronyms, abbreviations, and units of measure used in this document. Some acronyms used only in tables may be defined only in those tables.

### GENERAL ACRONYMS AND ABBREVIATIONS

AIM	Assessment, Inventory, and Monitoring
Argonne	Argonne National Laboratory
BLM	Bureau of Land Management
BSCI	biological soil crust index
CI	crust index
DOE	U.S. Department of Energy
DSM	digital surface model
DTM	digital terrain model
ERI	erosion resistance index
EVI	enhanced vegetation index
GNDVI	green normalized difference vegetation index
GPS	global positioning system
ISO	iterative self-organizing
LiDAR	Light Detection and Ranging
LTMP	long-term monitoring plan
MAE	mean absolute error
ME	mean error
MSAVI	modified soil-adjusted vegetation index
NDVI	normalized difference vegetation index
NHD	National Hydrography Dataset
NIR	near-infrared
NPV	nonphotosynthetic vegetation
PC1	first principal component
RMSE	root mean squared
RVI	ratio vegetation index

SEZ	solar energy zone
SVI	spectral vegetation index
USGS	U.S. Geological Survey
VARI	visible atmospherically resistant index
VHSR	very high spatial resolution

## **UNITS OF MEASURE**

cm	centimeter(s)
km	kilometer(s)
km <sup>2</sup>	square kilometer(s)
m	meter(s)
m <sup>2</sup>	square meter(s)
nm	nanometer(s)
μm	micrometer(s)

# **LONG-TERM MONITORING OF UTILITY-SCALE SOLAR ENERGY DEVELOPMENT AND APPLICATION OF REMOTE SENSING TECHNOLOGIES**

by

Yuki Hamada, Mark A. Grippo, and Karen P. Smith

## **EXECUTIVE SUMMARY**

In anticipation of increased utility-scale solar energy development over the next 20 to 50 years, federal agencies and other organizations have identified a need to develop comprehensive long-term monitoring programs specific to solar energy development. Increasingly, stakeholders are requesting that federal agencies, such as the U.S. Department of the Interior Bureau of Land Management (BLM), develop rigorous and comprehensive long-term monitoring programs. Argonne National Laboratory (Argonne) is assisting the BLM in developing an effective long-term monitoring plan as required by the BLM Solar Energy Program to study the environmental effects of solar energy development. The monitoring data can be used to protect land resources from harmful development practices while at the same time reducing restrictions on utility-scale solar energy development that are determined to be unnecessary. The development of a long-term monitoring plan that incorporates regional datasets, prioritizes requirements in the context of landscape-scale conditions and trends, and integrates cost-effective data collection methods (such as remote sensing technologies) will translate into lower monitoring costs and increased certainty for solar developers regarding requirements for developing projects on public lands. This outcome will support U.S. Department of Energy (DOE) Sunshot Program goals. For this reason, the DOE provided funding for the work presented in this report.

Argonne developed remote sensing methodologies for characterizing landscape features and properties and identified effective remote sensing metrics to support BLM's development of effective, financially sustainable long-term environmental monitoring strategies for desert regions of the Southwestern United States, where increased utility-scale solar development is anticipated in the coming decades. The effectiveness of remote sensing technologies, particularly very high spatial resolution (VHSR) imagery, was examined for three land resource categories: surface hydrologic features, vegetation, and soil (or surface). For vegetation and soil, the study focused on four of BLM's monitoring indicators for the Riverside East Solar Energy Zone (SEZ) pilot long-term monitoring plan (LTMP)—amount of bare ground, vegetation composition, vegetation height, and soil and site stability.

The algorithm for extracting ephemeral stream channels was developed by translating landscape associations into a series of spectral transformation and statistical operations. The algorithm is capable of extracting a range of channel types and mapped the distributions of ephemeral stream networks in much greater detail than the commonly used U.S. Geological Survey (USGS) National Hydrography Dataset (NHD) (USGS 2008). The algorithm detected 900% more ephemeral streams than were mapped in the study area in the NHD. The additional

detailed data about the ephemeral stream network would enhance local and landscape-scale hydrological modeling, which is necessary for monitoring the impacts of utility-scale solar development. The optimal remote sensing metrics for mapping vegetation distribution and fractional cover of vegetation types and bare ground were also identified, and vegetation height information was obtained from an image-derived point-cloud layer, a digital surface model (DSM), and a digital terrain model (DTM). Vegetation height was generally underestimated by 30 cm. The method reliably mapped fractional cover of two vegetation types and bare ground that indicated landscape composition. In addition, to accommodate the unique challenges in desert soil, a new remote sensing metric, the erosion resistance index (ERI), was developed, and the effectiveness of remote sensing metrics for estimating soil properties (e.g., moisture and organic matters) and biological soil crust distribution were investigated. While it is preliminary, ERI values reflected the erosive potential of the surface types examined in general. Although it was not feasible for this study because of the unavailability of reference data, a formal accuracy assessment that yields quantitative performance measures using appropriate validation data would provide conclusive evaluation of the remote sensing metric. Distribution of biological soil crusts was identified within a small range of biological soil crust index (BSCI). The effectiveness of that remote sensing metric is needed in order to draw conclusive outcomes.

At least six remote sensing metrics were shown to be effective for obtaining information about ephemeral stream channel networks, vegetation, and soil resources: spectral reflectance (i.e., red, green, and near-infrared bands), visible atmospherically resistant index, DSM, DTM, the principle component of the reflectance values, and ERI. In addition, three resource types shared a few common remote sensing metrics, and output for one resource type served as input for another resource type. This linkage suggests the possibility that independent remote sensing methodologies can be integrated into a single tractable workflow to optimize the efficiency of information extraction. If so, a single VHSR image would serve as a common data source for cost-effectively assessing multiple resources. The output from the remote sensing methodologies could also be used to study other resource types, such as vegetation patterns, which are indicative of the health and distribution of wildlife habitat. Thus, the remote sensing methodologies developed in this study can potentially be applied to monitoring a broad range of plant and animal resources.

Although the resource characterization methodologies described in this report show great promise for long-term monitoring applications, additional work is needed before integrating these remote sensing methodologies into BLM's long-term monitoring framework and/or into the monitoring plan required for an existing or planned utility-scale solar energy development. Because of changes in environmental conditions (e.g., sun angle and cloud cover) between image collection dates, it is essential to test the robustness of remote sensing algorithms across images from multiple dates. Therefore, several steps are necessary to facilitate the use of the remote sensing methodologies developed in this study. These include determining the (1) types and magnitude of environmental changes that can be detected and quantified using the methodologies, (2) robustness and sensitivity of the methodologies for anticipated natural environmental variability across a time series of remotely sensed images, and (3) required types and levels of image data preparation for automated, systematic analysis to produce consistent output.

In addition to being a cost-effective monitoring approach, the methods developed in this study could ultimately reduce soft-costs for developers by accurately characterizing the ecological resources at potential development sites, thereby potentially reducing permitting and mitigation costs and speeding up the siting process.

*This page intentionally left blank.*

## 1 INTRODUCTION

Given the current and anticipated future number of utility-scale solar energy projects, numerous federal agencies (e.g., the U.S. Department of the Interior Bureau of Land Management [BLM], National Park Service, and U.S. Fish and Wildlife Service) and nongovernmental organizations (e.g., The Nature Conservancy, The Wilderness Society, and Defenders of Wildlife) have identified a need to develop comprehensive long-term monitoring programs specific to solar energy development. The basis for their concern is that the nature and magnitude of adverse impacts of widespread deployment of utility-scale solar technologies are not well understood, particularly at the landscape or cumulative scale. It is intended that comprehensive long-term monitoring, if designed appropriately, will assist public land managers in assessing and responding to impacts.

Long-term monitoring of utility-scale solar energy projects is needed to evaluate (1) the actual direct, indirect, and cumulative impacts compared with predicted environmental impacts; (2) the effectiveness and/or appropriateness of measures taken to avoid or minimize impacts at the project site; and (3) the effectiveness of regional, compensatory mitigation investments. Information on these factors must be integrated into the project authorization programs, policies, and requirements that ensure development occurs in an environmentally responsible manner. That is, long-term monitoring data should support adaptive management of solar development (e.g., adjustments to operating conditions and mitigation measures). In addition, these data should allow for timely identification of adverse impacts to allow effective action to restore, rehabilitate, and prevent further damage to affected resources.

Federal agencies like the BLM have an obligation to manage lands to protect the full array of natural, cultural, and social resources and values on those lands. Increasingly, stakeholders are requesting that the agencies develop rigorous and comprehensive long-term monitoring programs. The BLM has committed to doing so as part of its new Solar Energy Program approved in 2012 (<http://blmsolar.anl.gov>). Long-term monitoring programs must be based upon scientifically valid protocols that quantify the effects of solar development, verify that those effects are associated with solar development rather than other sources of environmental change, support analysis of impacts at multiple scales, and maximize data- and cost-sharing opportunities. Such programs need to be designed specifically to meet agencies' objectives for resource management and renewable energy development. They should promote interagency coordination, as well as engagement with developers and other stakeholders. And, they must maximize investment of limited financial and staff resources in order to be sustainable.

Argonne National Laboratory (Argonne) has supported the BLM in its Solar Energy Program through preparation of the programmatic environmental impact statement (PEIS) (BLM and DOE 2012), which established 17 solar energy zones (SEZs) (i.e., areas of public lands prioritized for utility-scale solar development) across six southwestern states. Since issuance of the Solar Energy Program Record of Decision (BLM 2012), the BLM has engaged Argonne to develop and implement components of the new program, including regional mitigation strategies and long-term monitoring and adaptive management strategies. As part of this effort, Argonne is currently assisting the BLM in developing a pilot long-term monitoring plan (LTMP) for the

Riverside East SEZ, located in Riverside County, California. The monitoring objectives will focus on detecting landscape-level solar-related impacts on natural resources, as required by the Solar Energy Program Record of Decision. The Riverside East SEZ LTMP incorporates recommendations from BLM's Assessment, Inventory, and Monitoring (AIM) strategy for multiscale long-term monitoring on public lands. The AIM strategy identifies and emphasizes the importance of remote sensing, in addition to traditional field-based environmental monitoring methods, in meeting the significant data collection needs across expansive and remote public lands (Toevs et al. 2011). To assist the BLM in this effort, the U.S. Department of Energy (DOE) has concurrently funded Argonne's research of the application of remote sensing technologies for monitoring conditions in the desert environment surrounding the Riverside East SEZ.

In recent years, the use of remote sensing has become widespread, with emergent sensor and platform technologies and advanced modeling and data management infrastructure. While numerous remote sensing methodologies have been developed for collecting land surface information, there are unique challenges in applying remote sensing to desert environments. Desert landscapes are characterized by the scarcity of water, highly reflective soils, and sparse and less vigorous vegetation. This combination seems to violate fundamental assumptions in remote sensing, including (1) spectral reflectance signals from elements on the ground are isolated from environmental and instrumental noise, (2) targets are spectrally separable from background, and (3) different target types have unique spectral signatures (Friedl et al. 2001; Stow 1995). In addition, surface characteristics such as subtle topographical gradient and limited exposed soils make existing data collection and processing tools (e.g., Light Detection and Ranging [LiDAR] and soil stability index) inadequate for reliably characterizing monitoring indicators in desert regions. Therefore, there is a need to develop remote sensing methods applicable to monitoring environmental features in desert regions.

Resource managers are interested in monitoring desert landscapes using information that determines locations, abundance, spatial patterns of priority resources and key ecosystem components, as well as their status, condition, and trends, which are meaningful to land management decisions (Taylor et al. 2014). Sustainable and successful long-term monitoring methods will likely require the ability to cost-effectively collect information about multiple resource types or monitoring indicators. Characterizing many of the parameters indicative of resource types and monitoring indicators in desert regions, such as small plant canopies and narrow ephemeral stream channels, requires very-fine-scale remotely sensed data (e.g., < 50 cm). Very high spatial resolution (VHSR) multispectral images collected with high overlaps between adjacent image frames has a great potential to meet the requirements relatively inexpensively by (1) resolving fine-scale landscape features (e.g., shrub canopies and narrow ephemeral stream channels), (2) providing height information for vegetation and microtopography via an aerial triangulation technique, and (3) overlaying multiple data types (e.g., spectral and height information) with precise spatial and temporal fidelity. Thus, investigating the effectiveness of VHSR multispectral remote sensing for characterizing desert landscapes and developing VHSR remote sensing methodologies specific to desert environments are necessary to incorporate VHSR into BLM's sustainable, long-term solar energy monitoring strategies.

The goal of this project was to identify remote sensing metrics, using VHSR remotely sensed imagery, that are correlated with monitoring indicators and to develop cost-effective

remote sensing methods for detecting, identifying, and mapping land surface features and properties that are relevant for environmental monitoring. Cost-effectiveness is gauged in general terms in the context of developing methods that collect data sets across large areas of land more efficiently than traditional field-based methods and developing methods that use a single data set (VHSR) as opposed to multiple and more expensive remote sensing data types. To better support solar energy development on public land, the project focused on the three land resource types that correspond to ecosystem attributes emphasized in BLM's AIM strategy—surface hydrology, biotic integrity, and soils (or surface) (Toevs et al. 2011). Specific objectives were to (1) develop a cost-effective remote sensing methodology for mapping ephemeral stream networks in desert landscapes using VHSR multispectral imagery, (2) examine the effectiveness of VHSR remote sensing and of using spectral information to characterize vegetation distribution and land cover types in desert environments, and (3) explore spectral reflectance of the VHSR image and develop a new spectral index that would indicate erosion risks in desert environments. The cost-effective remote sensing methods developed for this study can be integrated into environmental monitoring programs such as the Riverside East SEZ LTMP, thereby meeting the needs of authorizing agencies, developers, and stakeholders.

*This page intentionally left blank.*

## 2 STUDY AREA

The study area is in the Palo Verde Mesa in eastern Riverside County, California (Figure 1). The area is a part of the Riverside East SEZ, the largest of the SEZs designated by the BLM (BLM and DOE 2012). The total area designated for utility-scale solar energy projects within the SEZ is 598.6 km<sup>2</sup>. As of September 2014, four solar projects had been authorized and three project applications were pending; these proposed projects cover an area of about 124 km<sup>2</sup>, which equates to approximately 21% of the SEZ.

The study area extends approximately 170 km<sup>2</sup> for the 2012 data collection and 90 km<sup>2</sup> for the 2014 data collection, both of which contain at least one solar energy project area. The area is primarily covered by bare ground, with sparsely distributed vegetation that consists of desert scrub species (e.g., creosotebush [*Larrea tridentata*] and desert sunflower [*Ambrosia dumosa*]), microphyll trees (e.g., blue palo verde [*Parkinsonia florida*] and ironwood [*Olneya tesota*]), and annual herbs. The area exhibits typical desert stream networks made up of single-thread and braided channels mixed with discontinuous forms. The ground surface primarily consists of erodible soils formed by silt and sand, desert pavement, and sparsely distributed biological soil crust. Approximately a quarter of the area to the west exhibits rugged topography—it has about 130 m of elevation gain from 185 to 315 m above mean sea level—and the rest of the study area has a subtle topographic gradient toward the foothills.

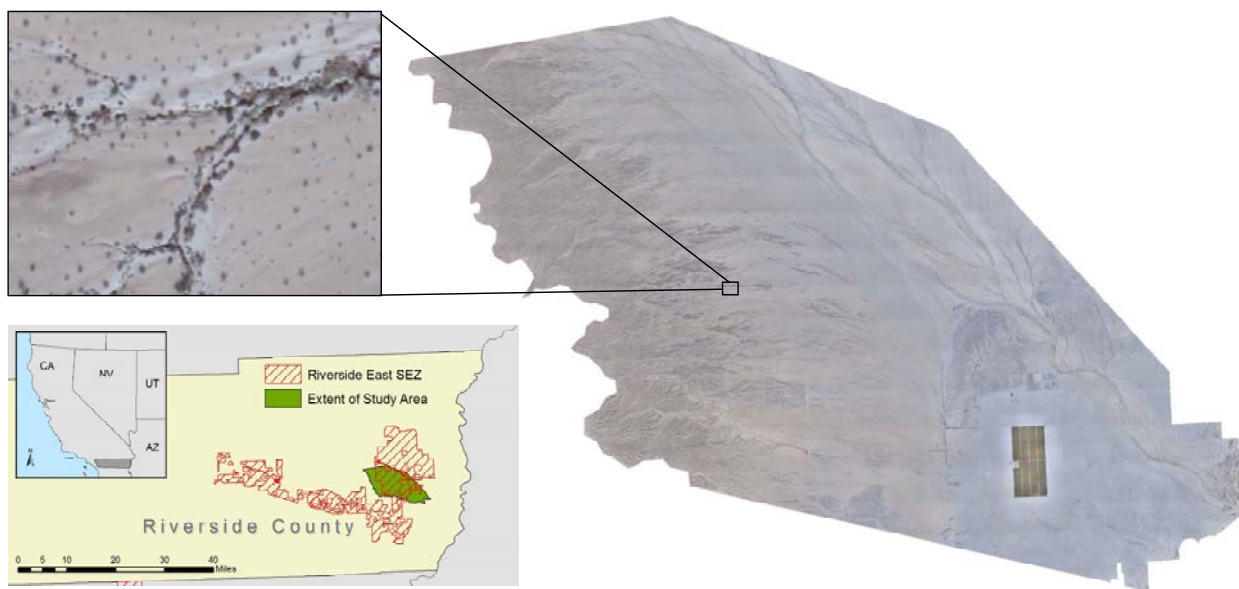


**FIGURE 1** Study Area (McCoy Wash, which runs in a northwest-southeast direction, is visible; it runs parallel to the northeast boundary of the study area. Irrigated fields are visible in the southeast corner of the study area.) The upper left hand inset image shows a close-up view of the ephemeral channels.

*This page intentionally left blank.*

### 3 METHODOLOGY OVERVIEW

#### 3.1 DATA

VHSR multispectral images of the study area were collected November 12 and 13, 2012, and January 15 and 16, 2014, using a lightweight fixed-wing sport aircraft approximately 1,350 m above the ground (Table 1). The VHSR images consist of four spectral bands within the visible and near-infrared (NIR) spectral regions and 15-cm spatial resolution. A total of 1,572 image frames were collected, with at least 50% forward image overlap and 60% side overlap, during the November 2012 flight; 2,699 frames were collected, with at least 85% forward overlap and 70% side overlap, during the January 2014 flight. For both flights, images were acquired between 11:30 a.m. and 1:30 p.m. to minimize illumination effects. The image frames were radiometrically corrected, mosaicked, orthorectified, and clipped to the study extent. For each data collection, a digital surface model (DSM) and a digital terrain model (DTM) were generated from the VHSR image frames having considerable spatial overlap using an automated aerial triangulation method by the vendor. Refinements of image collection specifications from the first to the second image collection resulted in DSMs and DTMs with varying spatial resolutions, 70 cm and 5.15 m for 2012 and 73 cm and 2.5 m for 2014, which were the finest horizontal scales attainable using the VHSR images with the image collection specifications.

Field data were collected on September 25 and 26, 2012, and January 21–23, 2014 (Table 2). Occurrence of vegetation and bare ground (e.g., exposed soil and desert pavement) and plant life-form types were observed during the 2012 field work at locations selected, based on accessibility and relative representativeness, and because of a lack of detailed knowledge about composition and spatial patterns of land cover types in the study area. During the 2014 field work, ground cover surveys were conducted at 19 sites along three 30-m transects configured in a spoke design that was suggested by Herrick et al. (2005). Canopy diameter was measured directly from each plant canopy or patch during 2012, and it was later calculated using canopy gap measurements for 2014. Cover and bare ground estimates were computed using both transect survey data for 2014 and using a dot-grid sampling method applied to the VHSR image mosaic (Duncan et al 1993; Hamada et al. 2010).

Although it was outside the scope of the project, spectral reflectance values were collected during the 2012 field work with in-kind support from the San Diego State University, Geography Department. The spectral reflectance data were primarily used to understand overall spectral characteristics of vegetation and bare ground and to calibrate the VHSR image data values into reflectance values. The spectral reflectance values were not collected during the 2014 field work largely because the data from the 2012 field work would serve as reference data for standardizing the 2014 dataset, but also because of budget and schedule constraints.

We planned to collect survey-grade global positioning system (GPS) data during the 2014 field work based on the insufficient positional accuracy of the hand-held GPS data from the 2012 field work. Because of unforeseen instrument malfunction during data collection and/or data transfer, we could not retrieve the data despite all possible attempts.

**TABLE 1 Summary of Remotely Sensed Data**

Specification	Dataset 1	Dataset 2
Date of image collection	November 12–13, 2012	January 15–16, 2014
Camera system	Canon 5D Mark II digital single-lens reflex camera (21-megapixel)	
Platform	Fixed-wing lightweight aircraft	
Time of data collection	11:30 a.m.–1:30 p.m.	
Forward/side overlap	60%/50%	85%/70%
Mean flight altitude	1,350 m	1,315–1,437 m
Total frames	1,572	2,699
Spectral band	Blue, green, red, near-infrared	
Image spatial resolution	15 cm	14.7 cm
Radiometric quantization	8 bit (orthorectified image) Floating point (DSM, DTM)	Floating point
Point-cloud data type	Not applicable	.XYZ
DSM spatial resolution	70 cm	73 cm
DTM spatial resolution	5.15 m	2.5 m
Extent	170 km <sup>2</sup>	90 km <sup>2</sup>
Coordinate system and projection	UTM N11, WGS84	
Data format	GeoTIFF	BigTIFF (orthorectified image mosaic) GeoTIFF (tiles, DTM, DSM)

Abbreviations: DTM = digital terrain model, DSM = digital surface model, UTM = Universal Transverse Mercator, N = north, WGS = World Geodesic System, TIFF = tagged image file format.

Using the field observation, additional locations of vegetation, exposed soil, and desert pavement were manually digitized in the VHRS imagery in order to generate sufficient reference data. This approach was taken because of the insufficient amount of observation due to time constraints and inclement weather during the fieldwork. The 15-cm resolution VHRS imagery was more than enough to resolve relatively small individual canopies in the scene, supporting reliable identification of vegetation and other land surface features across the landscape.

**TABLE 2 Summary of Field Survey and Sample Data**

	Dataset 1	Dataset 2
Date of survey	September 25–26, 2012	January 21–23, 2014
Ephemeral stream channel location	Recorded by walking along segments of ephemeral stream channels with a GPS device	Attempted to record using survey-grade GPS; not recorded due to instrument malfunction and/or data during data transfer
Vegetation occurrence	Recorded at selected areas; sampled using a dot-grid method applied to the VHRS imagery	Recorded using a line-point intercept method along three 30-m transects with a spoke design from preselected survey areas
Bare ground occurrence	Recorded at selected areas; sampled using a dot-grid method applied to the VHRS imagery	Recorded using a line-point intercept method along three 30-m transects with a spoke design from preselected survey areas
Occurrence of plant life-form type	Recorded at selected areas; sampled using a dot-grid method applied to the VHRS imagery	Recorded using a line-point intercept method along three 30-m transects with a spoke design from preselected survey areas
Vegetation height	Measured directly from canopies or patches at selected areas	Measured the tallest vegetating height within a 30-cm-diameter area at each location in a line-point intercept method
Canopy diameter	Measured directly from canopies or patches at selected areas	Calculated from the canopy gap survey (conducted using a canopy gap intercept method along the same transect above)
Spectral reflectance	Collected from vegetation and bright soil with the 380–1,000 nm (blue-NIR) spectral range using FieldSpec Pro (PANalytical Boulder).	Not collected
Field photo	Collected for vegetation and bare ground; served as ancillary data to aid confirmation of data and interpretation of results	Collected for vegetation and bare ground; served as ancillary data to aid confirmation of data and interpretation of results
Soil stability	Not collected	Collected from limited locations; found the method unsuitable for the study area due to lack of exposed surface soil and lack of soil aggregates
Soil sample	Not collected	Collected from two depths: 0–5 cm and 5–10 cm; analyzed for soil texture (% sand, % silt, and % clay), chemistry (% total carbon, % total organic carbon, % total inorganic carbon, and % total nitrogen), % moisture, and pH

## **3.2 DATA PROCESSING**

Table 3 shows the BLM's core and contingent monitoring indicators for which remote sensing metrics were considered in this study. In addition to the spectral bands, 12 remote sensing metrics and 1 transformation metric were examined for their effectiveness at characterizing surface hydrologic features, vegetation, and soil (or surface) in the study area. The monitoring indicators selected for this study were relatively amenable for remote sensing and were of interest to the Riverside East LTMP. The indicators included surface types (vegetation types and bare ground), vegetation height, photosynthesis, surface stability (indicative of soil aggregate stability), and soil properties such as texture and relative abundance of moisture, and organic carbon.

### **3.2.1 Extraction of Surface Hydrological Features**

A methodology was developed for extracting ephemeral stream networks from remotely sensed imagery on the basis of features associated with ephemeral channels that are recognizable to humans. Ephemeral stream channels are associated with relatively bright surface and dense, linear vegetation growth in the landscape. This simple association was translated into information about landscape features and structure that can be characterized using remote sensing (Figure 2, Conceptual Workflow). The landscape information was translated into a series of spectral transformation and spatial statistical operations using remotely sensed imagery in order to develop an image processing algorithm (Figure 2, Image Processing Workflow).

The algorithm was formulated to systematically analyze pixel values in the VHSR image to capture the landscape associations and map ephemeral channel features, as well as to delineate channel centerlines.

The modified soil-adjusted vegetation index (MSAVI) (Qi et al. 1994) was computed to characterize vegetation. To map vegetation canopies and patches, the minimum index value 0.14 (-1.4 standard deviation from the mean) was interactively determined and applied to the MSAVI layer. Vegetation density was calculated by applying a 5-m-radius circular moving window to the vegetation map in order to identify riparian corridors and characteristic vegetation patterns along narrow channels.

A principal component analysis was performed on the VHSR imagery. To enhance the characteristic brightness heterogeneity that resulted from the complex mixture of loose erodible soils and adjacent vegetation, local variability of the first principal component (PC1) layer was calculated using a 1.5-m-radius area.

The two layers that represent vegetation density and spatial heterogeneity of surface brightness were combined to generate a single-layer stack, which provided a physical basis for characterizing ephemeral stream channels, and 50 classes were generated on the basis of similarity in vegetation density and surface brightness heterogeneity. Classes in the output map that corresponded with ephemeral stream channels were identified by a visual comparison with

**TABLE 3 Monitoring Indicators and Relevant Remote Sensing Metrics Considered**

BLM Indicators <sup>a</sup>	Remote Sensing Metrics	Definitions	Reference
<i>Core indicators</i> <ul style="list-style-type: none"> <li>• Amount of bare ground</li> <li>• Vegetation composition</li> <li>• Non-native invasive species</li> <li>• Plant species of management concern</li> <li>• Vegetation height</li> <li>• Proportion of site in large intercanopy gaps</li> <li>• Land cover (habitat) amount, location, and pattern</li> <li>• Aquatic indicators</li> </ul>	Normalized difference vegetation index (NDVI)	$\frac{\rho_{NIR} - \rho_{red}}{\rho_{NIR} + \rho_{red}}$	Tucker 1979
	Green normalized vegetation index (GNDVI)	$\frac{\rho_{NIR} - \rho_{greem}}{\rho_{NIR} + \rho_{greem}}$	Unknown
	Visible atmospherically resistant index (VARI)	$\frac{\rho_{NIR} - \rho_{green}}{\rho_{NIR} + \rho_{green} + \rho_{red}}$	Gitelson et al. 2002
	Ratio vegetation index (RVI)	$\frac{\rho_{NIR}}{\rho_{red}}$	Unknown
<i>Contingent indicators</i> <ul style="list-style-type: none"> <li>• Soil and site stability</li> <li>• Soil toxins</li> <li>• Others (e.g., stand density index, wildlife metrics)</li> </ul>	Green-red ratio vegetation index (GRRVI)	$\frac{\rho_{green}}{\rho_{red}}$	Unknown
	Enhanced vegetation index (EVI)	$2.5 * \frac{\rho_{NIR} - \rho_{red}}{\rho_{NIR} + c_1 * \rho_{red} - c_2 * \rho_{blue} + L}$ $c_1 = 6, c_2 = 7.5, L = 1$	Huete et al. 2002
	Enhanced vegetation index 2 (EVI2)	$2.5 * \frac{\rho_{NIR} - \rho_{red}}{\rho_{NIR} + 2.4 * \rho_{red} + 1}$	Jiang et al. 1998
	Soil-adjusted vegetation index (SAVI)	$\frac{(\rho_{NIR} - \rho_{red}) * (1 + L)}{\rho_{NIR} + \rho_{red} + L}$ $L = 0.5$	Huete 1988
	Modified soil-adjusted vegetation index (MSAVI)	$\frac{2\rho_{NIR} + 1 - \sqrt{(2\rho_{NIR} + 1)^2 - 8(\rho_{NIR} - \rho_{red})}}{2}$	Qi et al. 1994
	Optimized soil-adjusted vegetation index (OSAVI)	$\frac{\rho_{NIR} - \rho_{red}}{\rho_{NIR} + \rho_{red} + 0.16}$	Rondeaux and Baret 1996
	Spectral reflectance values	Spectral reflectance values of the blue, green, red, and NIR spectral regions.	Not applicable

**TABLE 3 (Cont.)**

BLM's Indicators <sup>a</sup>	Remote Sensing Metrics	Definitions	Reference
	Crust index (CI)	$1 - \frac{\rho_{red} - \rho_{blue}}{\rho_{red} + \rho_{blue}}$	Karnieli et al. 1997
	Biological soil crust index (BSCI)	$\frac{1 - L \times  \rho_{red} - \rho_{green} }{(\rho_{green} + \rho_{red} + \rho_{NIR})/3}$ $L = 2$	Chen et al. 2005
	Principal components (PCs)	Orthogonal transformation of spectral reflectance values of blue, green, red, and NIR spectral bands.	Jensen 2000

<sup>a</sup> Source: Taylor et al. (2014).

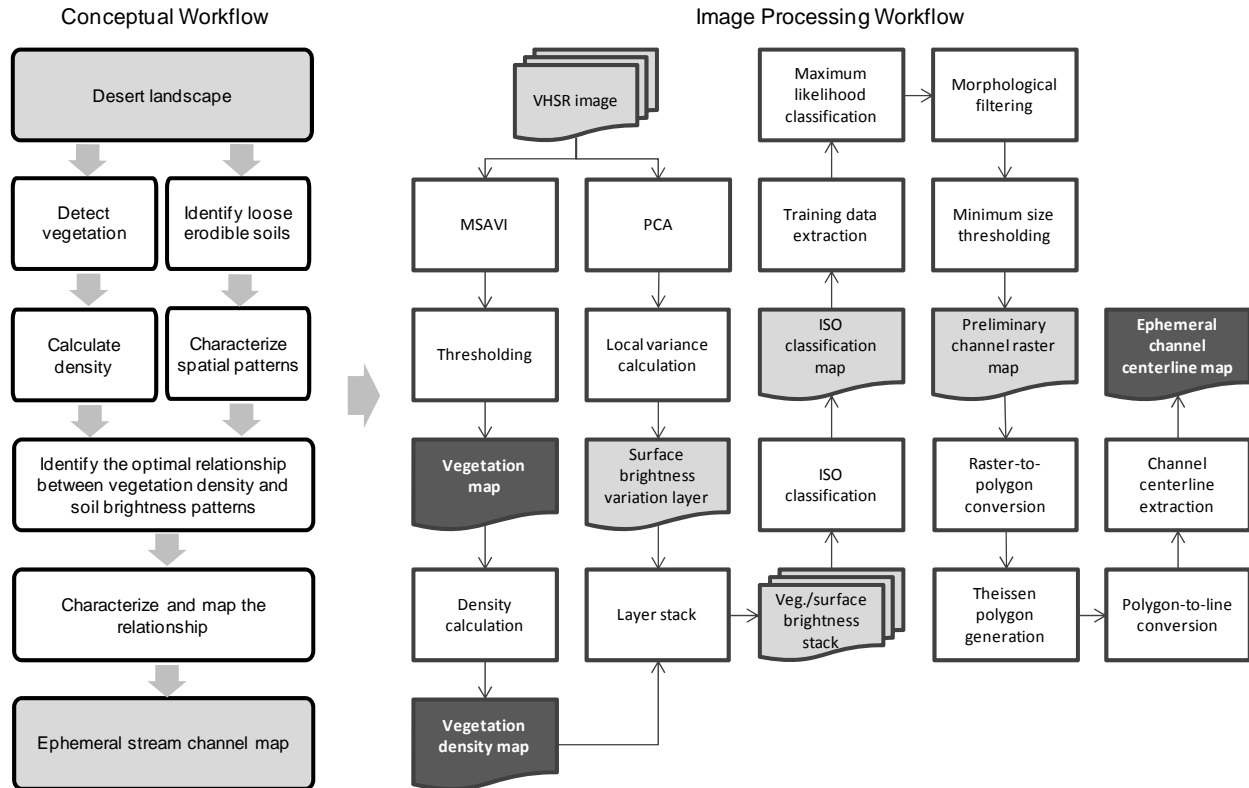


**FIGURE 2 Workflow Overview of Ephemeral Stream Channel Extraction Using Very High Spatial Resolution Multispectral Image (The output and intermediate products that could inform land and resource management decisions are shown in dark grey.)**

the reference map. Statistical properties of vegetation density and brightness heterogeneity were extracted from each of these classes to obtain training data in order to have comprehensive ephemeral stream channel characteristics with which to develop an algorithm. Using these training data, maximum likelihood classification was performed on the layer stack to generate a preliminary ephemeral stream channel map. To fill holes and remove isolated fragments in the map, a morphological closing operation with a 1.5-m-radius moving window was applied to the preliminary map. A cluster of candidate channel pixels smaller than 30,000 pixels (approximately 675 m<sup>2</sup>) was eliminated to exclude spatially incohesive clusters, and the final ephemeral channel classification map was generated. Having spatially incohesive clusters of pixels in remote sensing products is a typical consequence when using VHSR images. Minimum size filtering and majority filtering are the most commonly utilized image processing techniques for target detection and image classification, respectively.

To extract channel centerlines, the groups of pixels that represent ephemeral stream channels in the classification map were converted to polygons. The channel polygons were further converted to points, and additional vertices were generated every 5 m along the polygon edges. Thiessen polygons were then created around the channel edge vertices, creating a network of lines. Among the Thiessen polygons, edges corresponding to channels were identified, and centerlines of the channels, which were represented as one edge of the polygons, were extracted.

Irrelevant lines connecting to the centerline were removed to finalize the ephemeral channel centerline map.

Both ephemeral channel classification and centerline maps were examined to evaluate the performance of the algorithm for extracting stream channels in desert landscapes. Overall abundance and spatial patterns of the extracted channels in both maps were analyzed by comparing them with the National Hydrography Dataset (NHD) (USGS 2008). Quantitative analysis was performed using two 6-km<sup>2</sup> areas (or assessment areas) that contained varying drainage types in the landscape. For the classification map, accuracy metrics, including overall accuracy, producer's accuracy indicating a false negative,<sup>1</sup> and user's accuracy indicating a false positive were computed using more than 10,000 randomly selected pixels.

To evaluate the channel centerline map, the abundance and spatial distributions of channels were first qualitatively compared with the coarse-scale NHD to examine the level of detail the aerial remote sensing product represents. The local-scale accuracy of channel centerlines was evaluated based on the proportion of the length of the extracted channel to the length of the corresponding reference channel (i.e. 100% delineation means that extracted channel length equals reference channel length) represented the highest accuracy. The analysis included all channel segments longer than 150 m in both assessment areas. Then the number of reference channels with  $\geq 70\%$  and  $\geq 50\%$  of their channel delineated by the algorithm were identified and examined by independent analysts in order to determine whether the delineated channel centerlines could be visually recognized as channels regardless of the proportion delineated. To minimize bias, the independent analysts were not involved in developing the algorithm or generating the reference data. This qualitative method was employed in order to gain an understanding of the spatial patterns of extracted channel segments.

### **3.2.2 Vegetation Characterization**

#### **3.2.2.1 Characterization of Vegetation Distribution and Fractional Cover of Surface Types**

In support of two core monitoring indicators, amount of bare ground and vegetation composition, the development of remote sensing methods for vegetation characterization aimed to map accurate vegetation distribution and fractional cover of trees, shrubs, herbaceous plants (known as plant life-form or growth-form types), and bare ground (Table 3). The remote sensing methods strategically integrated a range of information that was derived from high-resolution multispectral imagery, including remote sensing metrics (known as spectral vegetation indices, or SVIs), DSM, and DTM (Figure 3). These spectral transformations and model were carefully examined and selected based on a rigorous, exhaustive analysis to optimize the characterization of desert vegetation.

---

<sup>1</sup> Producer's accuracy indicates how many targets in the reference data were correctly detected. User's accuracy indicates how many targets in the map product were actually present in the reference. If producer's accuracy is higher than user's accuracy, the map product tends to underestimate targets. If user's accuracy is higher than producer's accuracy, the map product tends to overestimate targets.

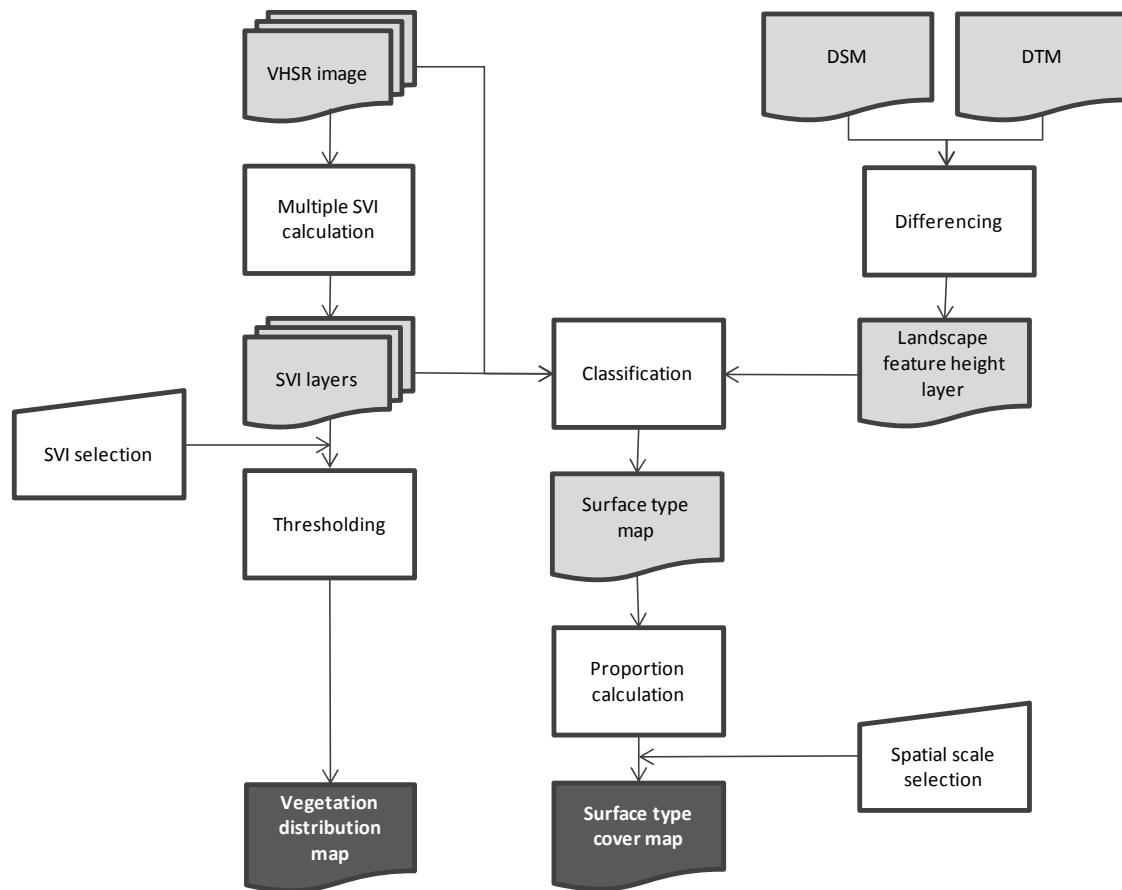


**FIGURE 3 Workflow Overview of Vegetation Distribution and Cover Estimation Using the Very High Spatial Resolution Multispectral Image (Output products are shown in dark grey.)**

A total of 10 SVIs that are widely used for vegetation studies (Table 3) were computed using the VHSR image mosaic. Nine small plots with known composition of surface types were selected, and their pixel values of vegetation were examined. The minimum threshold value was interactively selected for each SVI layer independently, and 10 vegetation maps were generated. Accuracy of the vegetation maps was assessed using more than 2,000 vegetation canopies and patches in three selected areas. In addition to visual assessment, kappa coefficient, false positive rate, and false negative rate were calculated as performance measures.

The optimal SVI, selected on the basis of the accuracy measures, was combined with the original VHSR image mosaic. Iterative self-organizing (ISO) classification (Tou and Gonzalez 1974) was performed to the combined-layer stack, and a total of 50 classes were identified based on the similarity in pixel values across layers. Among the resultant 50 classes, five ecologically/environmentally meaningful and spatially cohesive classes (or surface types)—vegetation, nonphotosynthetic vegetation (NPV), light soil, dark soil, and desert pavement—were identified based on the comparison with the VHSR image mosaic and field data. Training

data were extracted from at least 10 groups of pixels and correlated to the 4 surface types. Using the training data, maximum likelihood classification was performed for the entire extent.

A canopy height layer was generated by subtracting the DTM values from the DSM values. Height information was computed using only the 2014 data because of the insufficient overlap between frames in the 2012 data. The height layer was combined with the preliminary surface type map, and the vegetation class was separated into trees from shrubs. In the resultant surface type map, the light soil, dark soil, and desert pavement were merged into a single bare ground class according to BLM's AIM Program criteria (Toevs et al. 2011). The final map delineated trees, shrubs, NPV, and bare ground.

Fractional cover of each surface type was computed for a 15-m × 15-m area using the surface type map to accommodate to spatial scales of 30 m for our field data and 60 m recommended by the BLM AIM Program. Accuracy of fractional cover of surface types was examined using 10 rectangular plots. Mean error (ME), mean absolute error (MAE), and root mean squared error (RMSE) were calculated for all cover types to assess accuracy in cover estimates.

### **3.2.2.2 Estimation of Vegetation Height**

Vegetation height was estimated using two approaches: (1) plant height along the field survey transect and (2) the maximum height of individual plant canopies or patches (Figure 4). For both approaches, vegetation height was estimated from the image-based point-cloud data indicating height information, which were derived from the highly overlapped VHSR image frames (Table 1). The data values in the point-cloud data were interpolated to generate a spatially continuous layer.

To examine the effectiveness of the remote sensing approach for estimating plant height along transects, the field survey locations having vegetation height measurements were identified in the interpolated point-cloud layer. The minimum and maximum height values within a 1.5-m radius area were calculated for each point. Applying the small area for extracting minimum and maximum values provides elevation on the ground adjacent to a vegetation feature, as well as compensates for positional uncertainty in the survey points in the interpolated point-cloud layer. The minimum value was subtracted from the maximum value to obtain vegetation height for each of the survey locations. The vegetation-height estimates were compared with the recorded plant height to examine the potential for remote-sensing-based plant height estimation. Based on the data quality information provided by the vendor, the survey points having an estimated height < 6 cm were excluded from the validation. Out of remaining 49 survey points, 40 points were used to develop a linear function, and the function was applied to the whole interpolated point-cloud layer. ME, MAE, and RMSE were calculated using the 9 points that were not used to develop the function to assess the accuracy of the function.

To estimate plant height for vegetation features, height of individual plant canopies and patches was estimated using the interpolated point-cloud layer in conjunction with the vegetation layer generated in Section 3.2.2.1. Boundaries of vegetation polygons were expanded outward by

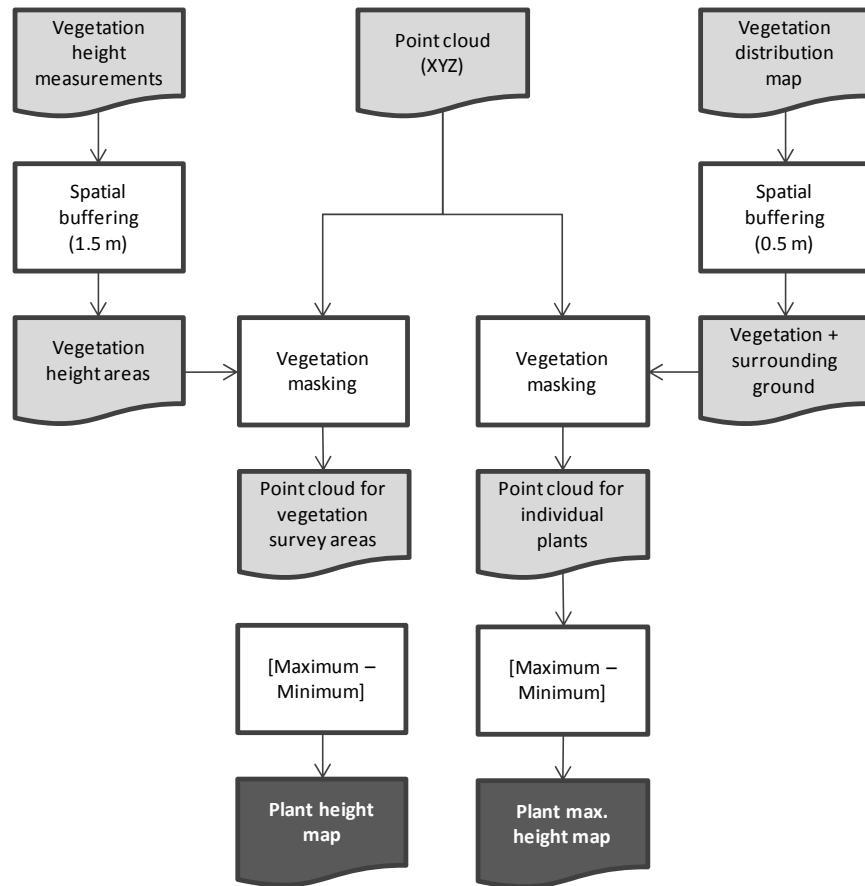


**FIGURE 4 Workflow Overview of Vegetation Height Estimation Using the Very High Spatial Resolution Multispectral Image (Output products are shown in dark grey.)**

50 cm in order to include ground around the canopies and patches. For each expanded polygon, the minimum and maximum values of the interpolated point-cloud layer were extracted. The minimum and maximum values of each polygon were assumed to correspond to surface elevation and elevation at the highest point of each vegetation feature, respectively. Vegetation height was obtained by subtracting the minimum value from the maximum value. Because validation data were unavailable, only qualitative assessment was performed based on visual interpretation of the output.

### 3.2.3 Surface Stability and Soil Properties

#### 3.2.3.1 A New Remote Sensing Metric for Assessing Soil and Site Stability, the Erosion Resistance Index

Bare ground, the primary surface type of the study area, consists of a mixture of soil (e.g., sand and silt), gravel of varying size and color, and rock fragments. The method for measuring soil stability recommended in the AIM protocols was developed for grassland, shrubland, and savanna ecosystems (Herrick et al. 2005) and was not effective for most of the desert bare ground surveyed during the 2014 field work. This prevented direct comparison between soil stability and remote sensing metrics. Therefore, a new remote sensing metric (or spectral index) was developed that would indicate surface stability, which equates to the risk of erosion of desert landscape land surfaces.

Spectral reflectance values of the 2012 VHSR image set were extracted from six surface types: stream beds mostly covered with loose sandy soil and silt that were deposited by surface runoff, unpaved roads dominated by sand that was mechanically disturbed by traffic, desert scrublands, bare ground containing noticeable gravels/rock fragments, disturbed desert pavement, and intact desert pavement. These surface types were expected to correspond to a gradient of surface stabilities ranging from low (stream beds) to high (desert pavement). Two-dimensional scatter plots were generated using all possible pairs of spectral band-ratios, and the band-ratio combination that exhibited the greatest separability between the surface types was identified. A new index of surface stability, the erosion resistance index (ERI), was derived by applying simple trigonometry to the band-ratio combination in order to identify the upper bounding line of the scatter plot, which corresponded to the most stable surface type. The perpendicular distance from the upper bounding line was calculated using the geometric equation developed by Perry and Lautenschlager (1984):

$$ERI = \frac{([b \times \frac{\rho_1}{\rho_2}] - \frac{\rho_3}{\rho_4} + a)}{\sqrt{b^2 + 1}}, \quad (1)$$

where  $a$  is the intercept of the upper line, and  $b$  is the slope of the upper line. The values  $\rho_1$ – $\rho_4$  are reflectance values of the VHSR imagery at given spectral bands. The equation was applied to the entire image, and the ERI was computed using both the 2012 and 2014 image sets. To evaluate the index, ERI values were extracted from areas of known surface types. At least 26 locations were sampled for each surface type. The ERI values were plotted by surface type, and summary statistics of the ERI values for each surface type were calculated. Box plots were generated to visualize overlap and/or separability between surface types.

Of all scatter plots of possible pairs of spectral band-ratios, the plot of the red/NIR band-ratio versus the green/red band-ratio showed the best separation between the surface types, that is, stream beds and unpaved roads, desert scrublands, bare ground with gravels, disturbed desert pavement, and intact desert pavement (Figure 5). The data space consisted of a lower line corresponding to the surface types that are most resistant to erosion (e.g., desert pavement) and

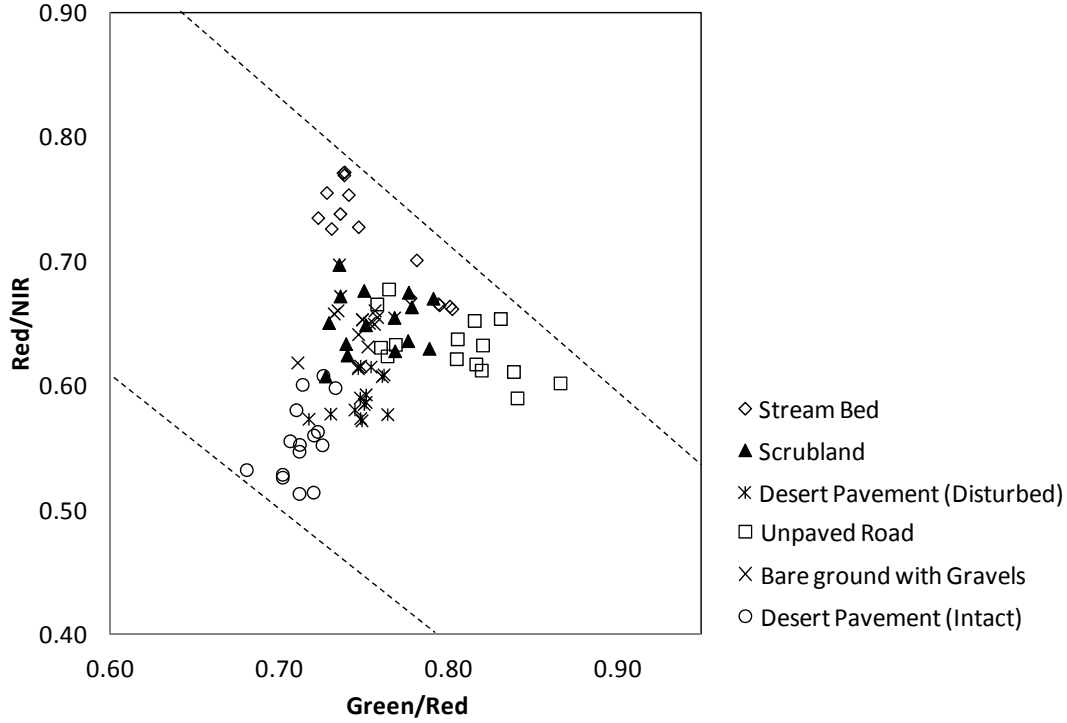


**FIGURE 5 Scatter Plot of a Green/Red Band-Ratio versus a Red/NIR Band-Ratio by Surface Type for Correspondence to a Range of Erosion Risks**

an upper line representing the most erodible surface materials (e.g., stream beds and unpaved roads). Applying Equation 1, the index was formulated as:

$$ERI = \frac{\left( \left[ -1.257 \times \frac{\rho_{green}}{\rho_{red}} \right] - \frac{\rho_{red}}{\rho_{NIR}} + 1.698 \right)}{\sqrt{-1.257^2 + 1}}, \quad (2)$$

where  $\rho_{green}$ ,  $\rho_{red}$ , and  $\rho_{NIR}$  are reflectance values of the green, red, and NIR spectral bands, respectively.

### 3.2.3.2 Soil Properties and Remote Sensing Metrics

Optical remote sensing is not typically used to investigate soil properties because electromagnetic radiation in the spectral range penetrates only 50  $\mu\text{m}$  of surface soil. Thus, there is no precedent study for such an application. Compared with soils in other ecosystems, such as forests and wetlands, desert soil would be relatively stable or change relatively slowly. Surface characteristics (e.g., abundance of vegetation, plant litter, and gravels) that are attainable using optical remote sensing may indicate subsurface soil properties. Therefore, exploratory statistical analysis was conducted with the premise that if any relationships were found, a hypothesis could be constructed and the soil sampling method could be amended as needed.

Two spatial scales, 15 cm and 1.5 m, were used to investigate the potential of VHSR remote sensing for studying soil properties. The original VHSR image mosaics from November 2012 and January 2014 were spatially aggregated into 1.5 m by averaging pixel values over a 1.5-m  $\times$  1.5-m area in order to compensate for high-frequency noise typical in high-resolution imagery. The following properties were computed using the 1.5-m resolution image remote sensing metrics: biological soil crust index (BSCI), crust index (or cyanobacteria index, CI), MSAVI, ERI, PC1, PC2, spatial heterogeneity of PC1 and PC2 within a 3-m-radius area, and vegetation density within a 5-m-radius area. Spectral reflectance values of the blue, green, red and NIR bands; the eight remote sensing metric values indicated in Table 3; and image-derived vegetation density were extracted from the soil sampling locations during the 2014 field work.

A total of nine soil properties were examined, including percentage moisture, percentage total carbon, percentage total organic carbon, percentage total inorganic carbon, percentage total nitrogen, percentage sand, percentage silt, percentage clay, and pH. The soils parameters were available at two depths, 0 to 5 cm (shallow, 12 sample locations) and 5 to 10 cm (deep, 8 sample locations) only from January 2014. These soil parameters were analyzed with the 2012 and 2014 remote sensing metrics because desert soil conditions do not change rapidly enough to be significantly different over a 2-year period. The inadequate sampling size and the lack of soil properties measurements in 2012 limited us to performing the task as an exploratory analysis.

Among the data, an outlier was identified using a matrix of correlation scatter plots. This outlier was excluded from further analysis following confirmation that its geographic location was inaccurate. Using the remaining data, Pearson and Spearman correlation matrices were produced for four stratified datasets independently: shallow soil at the 15-cm scale, shallow soil at the 1.5-m scale, deep soil at the 15-cm scale, and deep soil at the 1.5-m scale. For each stratified data set, the correlation outputs were grouped into one of the following categories: very weak ( $-0.19$  to  $0.19$ ), weak ( $-0.39$  to  $-0.20$ ;  $0.20$  to  $0.39$ ), moderate ( $-0.59$  to  $-0.40$ ;  $0.40$  to  $0.59$ ), strong ( $-0.79$  to  $-0.60$ ;  $0.60$  to  $0.79$ ), or very strong ( $-1.00$  to  $-0.80$ ;  $0.80$  to  $1.00$ ). For remote sensing metrics that showed strong and very strong correlations, the significance of their relationship was tested using a simple t-statistic. For those indicating strong or very strong correlations, functions to predict the soil properties were developed using the remote sensing metrics. For the linear relationships, simple linear regression was used. For the relationships that were identified as nonlinear but monotonic, simple linear regression was conducted on the log-transformed variables.

### **3.2.3.3 Biological Soil Crust and Remote Sensing Metric, the Biological Soil Crust Index**

BSCI (Chen et al. 2005) was computed using the January 2014 image mosaic (Table 1). Three locations that contain biological soil crust were used for the analysis. The locations selected during the 2014 fieldwork contained sparsely distributed cyanobacteria-dominant biological soil crust, which was typical of biological soil crust distribution in the study area (Nagy et al. 2005). BSCI values were extracted from total of 27 pixels (i.e., one set of nine pixels at each of the three locations): one pixel at the center of each location plus eight surrounding

pixels. Summary statistics were calculated from each location for each dataset. The BSCI layer was classified into five classes that would correspond to likelihood of biological soil crust occurrence using the following thresholds:  $< -10\%$  of the sample BSCI range (BSCI  $< 3.05$ ),  $\geq -10\%$  of the sample BSCI range (BSCI = 3.05-3.09), minimum and maximum values of sample data (BSCI = 3.09–3.54),  $\leq +10\%$  of the sample BSCI range (BSCI = 3.54—3.58), and  $> +10\%$  of the sample BSCI range (BSCI  $> 3.58$ ).

*This page intentionally left blank.*

## 4 RESULTS AND SYNTHESIS

### 4.1 SURFACE HYDROLOGIC FEATURES

The algorithm identified a large number of narrow ephemeral stream channels at the landscape scale across the study area (Figure 6). The channel classification map indicated the accurate identification of McCoy Wash, the largest stream feature, extending northwest to southeast of the study area (Figure 1). Numerous narrow tributaries occurred along the hill slope on both sides of the wash. The algorithm captured a range of channel widths and forms in both the west and east assessment areas. Underclassification (or false negatives) was often observed near stream headwaters and areas characterized by braided channel networks; overclassification (or false positives) often occurred around wide channels.

The majority of accuracy measures (i.e., overall, producer's, and user's) exceeded 75% across the assessment areas (Table 4), which is considered more than satisfactory for a fully automated procedure. Accuracy ranged from 48.5% to 91.8%. Producer's accuracy was higher than user's accuracy in both areas, which indicated false positive detection or overclassification in the ephemeral channel map. This overclassification was intentionally created during the raster processing as a part of the strategy for increasing the connectivity of ephemeral stream channels during the channel centerline extraction.

A considerable number of channel centerlines were delineated by the algorithm across the study area (Figure 6). The algorithm detected 900% more ephemeral streams than were mapped in the study area in the NHD. Channel centerlines of McCoy Wash and other major tributaries were correctly delineated. Minor or narrow channels and those occurring in areas with even, sparse vegetation growth were frequently undetected. Channel features near stream headwaters were often missing from the final channel map. Although the algorithm correctly delineated wide channels consisting of well-defined braided forms, it exhibited difficulty delineating wide channels with single-threaded forms when they contained heterogeneous vegetation growth.

The difference between channel length delineated by the algorithm and that present in the reference data varied by the assessment areas (Table 4). The difference ranged from 8% for the east area in the November 2012 data to 27% for the west area in the January 2014 data. While the extracted channel areas were generally similar to the reference channel areas, approximately 45% fewer channels were extracted compared with the reference data. This considerable discrepancy in channel length was mostly explained by the differences between the reference data and algorithm in how channels were defined. For example, a wide tributary consisting of braided channels separated by a small distance may be delineated as multiple channels in the reference data, but may be identified as a single broad channel by the algorithm. Surface patterns across desert scrublands that were created by unstructured surface low or sheet-flow may be defined as channels in the reference data but may not be recognized as channels by the algorithm because of the lack of typical characteristics of ephemeral channels. Establishing a definition of ephemeral stream channels that are meaningful

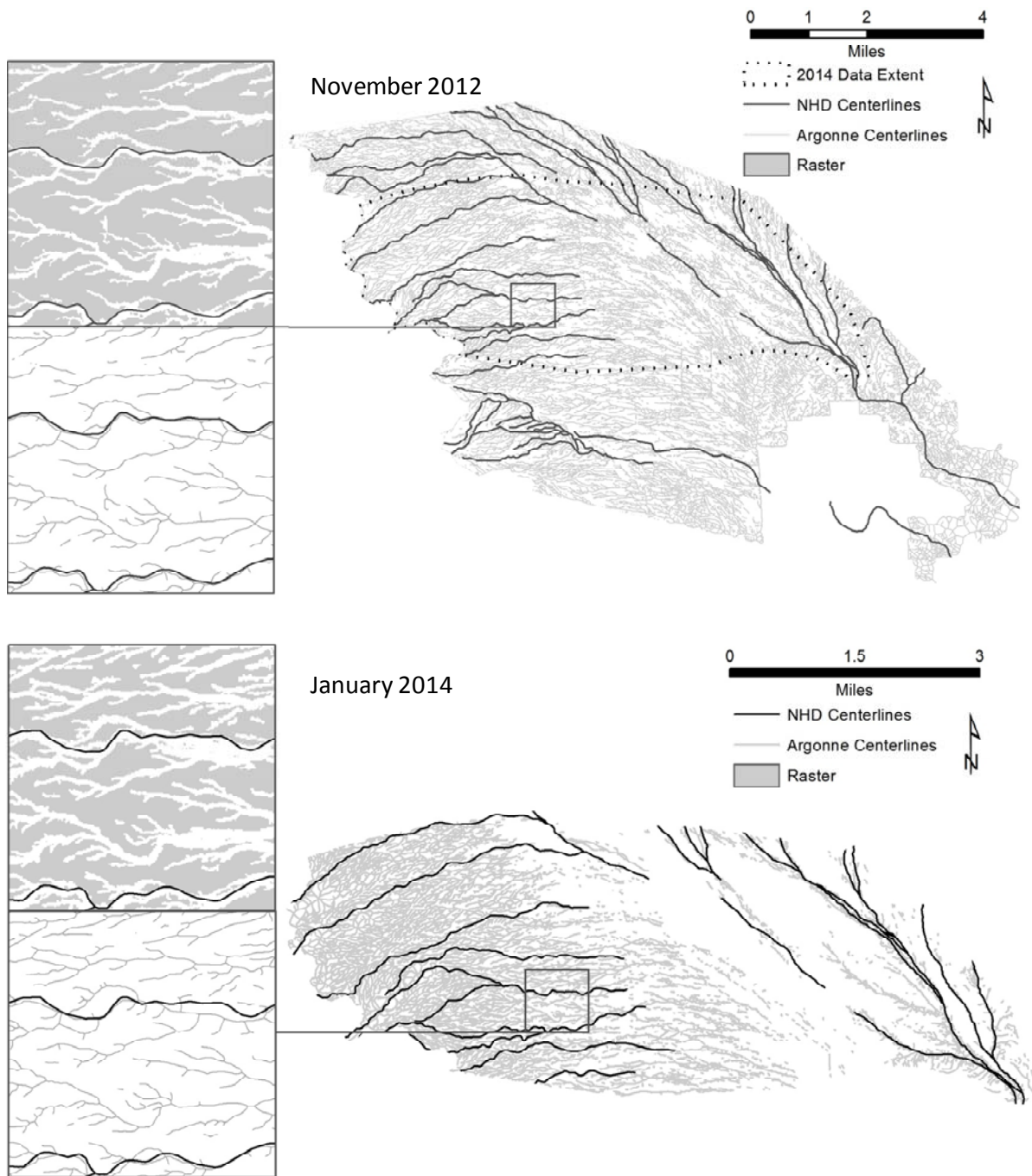


**FIGURE 6** Maps of Ephemeral Stream Channels Derived from the Very High Spatial Resolution Image Overlain with the NHD (McCoy Wash, which runs in a northwest-southeast direction, is visible running parallel to the northeast boundary of the study area.)

**TABLE 4 Accuracy of Ephemeral Stream Channel Maps Derived from Remotely Sensed Imagery**

<i>Classification Accuracy</i>						
	November 2012			January 2014		
	Pooled	West	East	Pooled	West	East
Overall accuracy (%)	77.0	91.1	79.8	79.9	72.2	86.8
Producer's accuracy (%)	85.8	91.8	88.2	86.8	99.6	84.8
User's accuracy (%)	52.2	48.5	51.4	51.6	18.0	79.1

<i>Centerline Extraction Accuracy</i>						
Length Delineated	November 2012*			January 2014*		
	Pooled	West	East	Pooled	West	East
Total channel length (km)	146.0	50.9	95.1	79.5	51.6	27.9
	(154.0)	(66.3)	(87.7)	(96.2)	(70.8)	(25.4)
Accurate channel area (km <sup>2</sup> )	2.0	0.8	1.2	1.0	0.4	0.6
	(2.7)	(1.3)	(1.5)	(1.0)	(0.4)	(0.5)
Accurate channel length (km)	92.3	37.7	54.6	44.0	28.8	15.2
	(153.7)	(66.0)	(87.7)	(96.2)	(70.8)	(25.4)
Channel density (km/km <sup>2</sup> )	8.5	6.4	9.7	10.4	10.5	10.3
	(13.3)	(11.2)	(15.3)	(21.5)	(25.8)	(17.28)
Average channel width (m)	33.7	19.7	47.6	31.6	16.9	46.3
	(32.0)	(18.1)	(45.9)	(19.1)	(4.3)	(33.9)
Accurate delineation $\geq 70\%$ (%)	56.3	53.0	59.5	38.1	38.6	37.5
Accurate delineation $\geq 50\%$ (%)	66.5	65.5	67.5	60.9	84.2	37.5
Recognized (%)	89.0	86.0	92.0	87.4	89.5	87.5

\* Values in parentheses indicate reference data.

for ecological and management perspectives (e.g., active versus inactive, a single aggregated tributary versus a set of individual braided channels) is needed in order to generate reliable reference data and to refine the algorithm. This would help provide valuable detailed distributions of ephemeral stream channels for local or landscape-scale hydrological modeling and inform resource management decisions.

The accuracy of the channel width estimated was considerably different between the 2012 and 2014 datasets. While channel width was estimated with approximately 5% error for the 2012 data, channel width for the 2014 data was overestimated by approximately 130% of the reference data (Table 4). This overestimation is more significant for the west assessment area than the east area. This considerable overclassification (or false positive) indicated as very low user's accuracy for the January 2014 classification has resulted in significant overestimation of

channel width for the assessment area. The recalibration of the algorithm based on the 2014 data, which had higher quality than the 2012 data, would mitigate the discrepancy.

Within the west and east assessment areas,  $\geq 70\%$  and  $\geq 50\%$  of channel lengths were delineated for more than a half of the reference channel segments in most cases examined with some exception (e.g., delineation  $\geq 70\%$  for the January 2014 data) (Table 4). For the 2012 data, the two assessment areas showed nearly identical accuracy in channel centerline delineation while centerline delineation accuracy for the west area was considerably higher than for the east area in the 2014 data. The discrepancy in accuracy of the east area may be due to edge-effects that stemmed from the insufficient image coverage in the 2014 data. The assessment area was defined based on the 2012 image extent. The 2014 image did not fully include the east assessment area because of the adjustments/optimization of image collection parameter prior to the 2014 image collection. Although the accuracy calculation for the 2014 data was only limited to its image extent, the influence of potential edge-effects was inevitable.

In contrast to the modest accuracy of the criteria-based assessment, which is defined by percentage of length of the delineated channel, the analyst-based method indicated that approximately 90% of the reference segments were correctly extracted based on the combination of the delineated channel lengths in each segment and the distribution or delineated line fragments within a validation segment. For example, when 40% of the channel length for a reference segment was delineated by the algorithm, the segment detection was not considered a success based on the 70% or 50% criterion. However, it may have been considered a success in the analyst-based assessment when the analyst recognized the segment from the delineated centerlines, which may consist of small channel fragments linearly distributed across the validation segment. This high recognition rate result suggests that the channel segments extracted using the algorithm were spatially cohesive and had strong association with ephemeral stream channels present in the study area. This result indicates that inclusion of a pattern recognition routine to the algorithm could further improve channel extraction accuracy, as well as effectiveness of the current algorithm.

## **4.2 CHARACTERIZATION OF VEGETATION AND VEGETATED SURFACE**

### **4.2.1 Vegetation Distribution and Fractional Cover of Surface Types**

Vegetation maps generated from SVIs accurately characterized vegetation distributions in desert lands (Figure 7). There were two distinct patterns exhibited in a riparian habitat type. The normalized difference vegetation index (NDVI), green normalized vegetation index (GNDVI), and visible atmospherically resistant index (VARI), which apply a normalized difference ratio using varying band combinations, showed nearly identical detection patterns and tended to slightly overestimate vegetation. The rest of the SVIs tended to underestimate vegetation cover, particularly for shaded parts of canopies. In areas having vegetation over desert pavement, GNDVI, VARI, and the ratio vegetation index (RVI) accurately detected vegetation. Pronounced overestimation was observed in the maps derived from NDVI and enhanced vegetation index (EVI). GNDVI and VARI appeared to perform best among the SVIs tested.

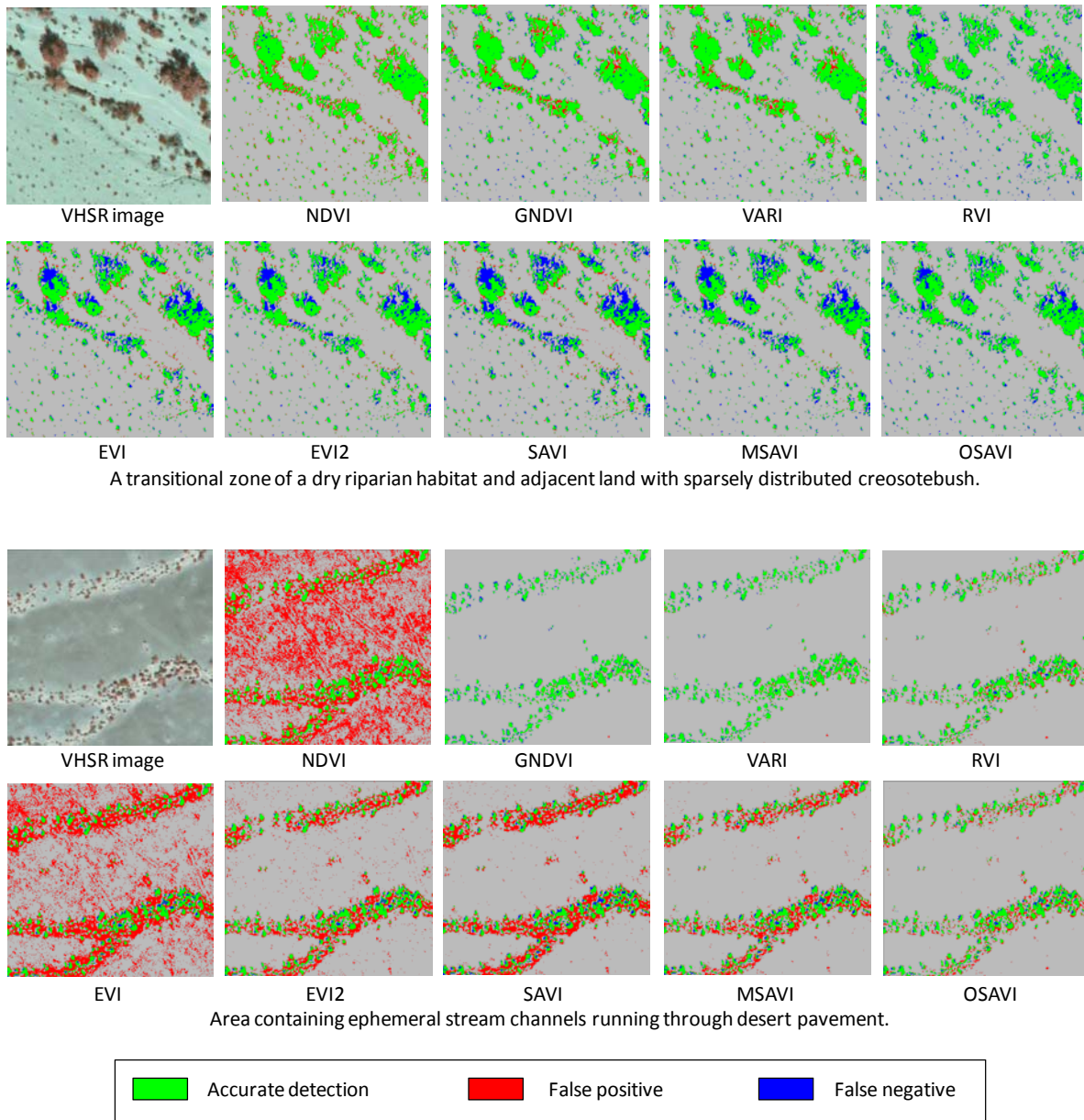


**FIGURE 7 Close-Up Views of Vegetation Distribution Maps Derived from the Very High Spatial Resolution Image**

Kappa values ranged from 0.69 to 0.88 and from 0.36 to 0.87 for the November 2012 and January 2014 image mosaics, respectively (Table 5). Most SVIs performed considerably better than random assignment, as kappa values were much greater than 0.5 (exceptions were NDVI, RVI, and EVI). Between the two image sets, detection accuracy was higher in the November 2012 products (average kappa = 0.825) than that in the January 2014 products (average kappa = 0.648), which may be influenced by the phenology of landscape due to the difference in the image collection season. Regardless of the image set, SVIs often overestimated vegetation, as indicated by the higher false positive rate than false negative rate. While a number of SVIs

**TABLE 5 Accuracy of Vegetation Distribution Map Derived from Remotely Sensed Imagery**

Metric	NDVI	GNDVI	VARI	RVI	EVI	EVI2	SAVI	MSAVI	OSAVI
November 2012									
Threshold value	0.19	0.27	0.24	1.61	0.15	0.16	0.28	0.15	0.16
Kappa	0.85	0.69	0.87	0.78	0.78	0.88	0.84	0.87	0.87
False positive	24.6%	46.5%	16.1%	12.1%	34.2%	10.8%	16.5%	16.8%	17.7%
False negative	3.5%	1.0%	14.1%	14.3%	4.2%	13.5%	15.4%	9.0%	6.6%
January 2014									
Threshold value	0.13	0.34	0.22	1.45	0.11	0.11	0.22	0.12	0.13
Kappa	0.53	0.87	0.85	0.36	0.36	0.71	0.63	0.71	0.80
False positive	63.1%	14.1%	14.0%	9.5%	70.8%	34.5%	41.1%	28.8%	16.1%
False negative	3.3%	11.9%	10.3%	19.0%	51.6%	22.0%	32.8%	29.3%	22.9%

Abbreviations: NDVI = normalized difference vegetation index, GNDVI = green NDVI, RVI = ratio vegetation index, GRRVI = green-red ratio vegetation index, EVI = enhanced vegetation index, SAVI = soil-adjusted vegetation index, MSAVI = modified soil-adjusted vegetation index, OSAVI = optimized soil adjusted vegetation index.

clearly performed better in the 2012 image than in the 2014 image, VARI performed well for both image sets according to all three measures (Kappa = 0.86; false positive = 15.0%; and false negative = 12.2%). VARI is superior to GNDVI because its accuracy was more consistent between the two data collection dates than that of GNDVI (e.g., Kappa = 0.87 and 0.85 for VARI and kappa = 0.68 and 0.87 for GNDVI). In addition, threshold values of VARI from the two datasets differed by only 0.02; this indicates that the index is stable for detecting vegetation in dry lands, as well as robust in various environmental conditions in desert regions. On the basis of both these qualitative and quantitative assessments, VARI would be the optimal vegetation index for mapping vegetation distribution in our study area, and possibly other desert regions.

Fractional cover of the four surface types is shown in Figure 8. Overall, bare ground was the dominant cover type in the study area, and the four surface types exhibited different abundance and spatial distributions across the landscape. Relatively high vegetation cover formed linear features in the west-east direction, which appear to follow along ephemeral stream channels in the study area. Tree cover was greater along the upstream riparian habitats located in the southwest (or lower left quadrant). While shrub cover was evenly distributed over the landscape with a relatively systematic pattern, a greater cover of NPV was present in areas from the north and northwest to west (or top to left half of the area).

The remote sensing method estimated fractional cover accurately, with error less than 9% across nearly all plots, except for Plot 7, which overestimated NPV and underestimated bare ground by 22.2% and 28.9%, respectively. Overall error was considerably reduced by excluding Plot 7 from the analysis. The ME indicated a shift in overall trend in error for NPV estimation from positive (overestimation) to negative (underestimation). MAE and RMSE were

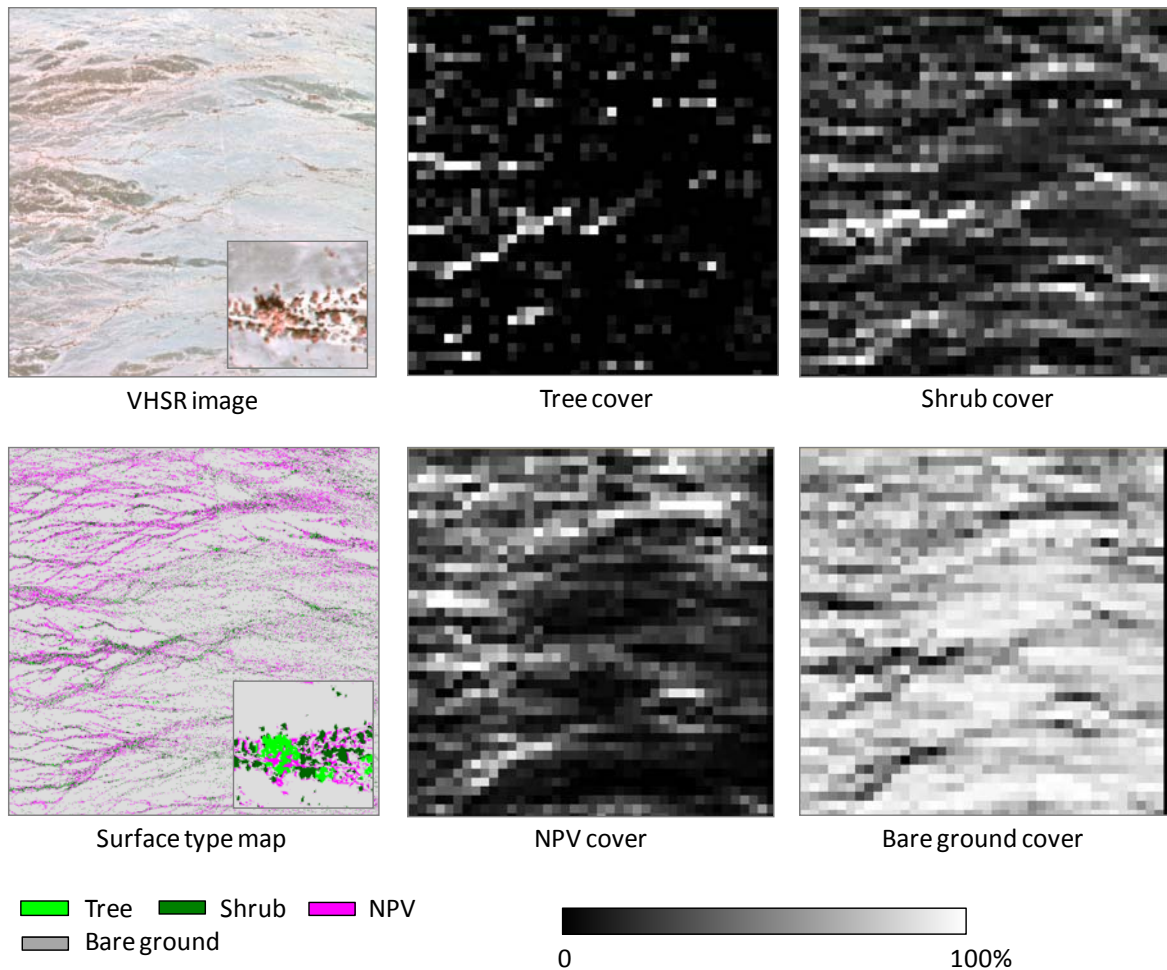


**FIGURE 8 Close-Up Views of Fractional Cover Maps of Surface Types Derived from the Very High Spatial Resolution Image**

approximately 2% lower for NPV and bare ground, and RMSE of bare ground noticeably dropped from 20.8% to 6.0% when excluding Plot 7 from calculation.

Plot 7 was located in a large, less defined wash that exhibited mixed ground color (Table 6). Some portion of bare ground resembled dry plant litter and/or senesced herbaceous plants at the time of image collection. This spectral similarity likely caused confusion in classification and resulted in the misclassification of bare ground as NPV. Differentiating NPV from background soil is often challenging when mapping land cover in arid and semiarid environments (Hamada et al. 2011, 2013; Okin et al. 2001). The confusion between senesced herbaceous plants and bare ground may be alleviated by collecting imagery shortly after a rain event when herbaceous plants are more photosynthetically active.

The SVIs appeared to have slightly underestimated trees and shrub cover. Underestimation of trees often resulted from less illuminated tree canopies being classified as shrubs. Underestimation of shrubs was caused by bare branches or portions of canopies having

**TABLE 6 Accuracy of Surface Type Fractional Cover Maps Derived from Remotely Sensed Imagery**

Plot	Reference				Remote Sensing Estimate (RSE)				RSE – Reference			
	Tree (%)	Shrub (%)	NPV (%)	Bare (%)	Tree (%)	Shrub (%)	NPV (%)	Bare (%)	Tree (%)	Shrub (%)	NPV (%)	Bare (%)
1	3.1	12.5	12.5	71.9	2.5	7.6	15.4	72.1	-0.6	-4.9	2.9	0.2
2	4.7	12.5	20.3	62.5	5.0	7.9	16.9	67.9	0.3	-4.6	-3.4	5.4
3	7.8	3.1	9.4	79.7	3.3	5.0	4.9	85.6	-4.5	1.9	-4.5	5.9
4	0.0	10.9	4.7	84.4	0.1	6.6	3.3	88.2	0.1	-4.3	-1.4	3.8
5	0.0	10.9	9.4	79.7	0.0	8.0	2.9	86.3	0.0	-2.9	-6.5	6.6
6	0.0	14.1	6.3	79.7	0.0	9.5	3.2	86.2	0.0	-4.6	-3.1	6.5
7	0.0	3.1	10.9	85.9	0.0	7.8	33.1	57.0	0.0	4.7	22.2	-28.9
8	0.0	10.9	9.4	79.7	1.6	4.2	5.0	88.3	1.6	-6.7	-4.4	8.6
9	0.0	3.1	14.1	82.8	0.0	2.0	18.5	79.2	0.0	-1.1	4.4	-3.6
10	0.0	10.9	3.1	85.9	0.1	3.0	1.9	94.2	0.1	-7.9	-1.2	8.3

---

	All Plots				Excluding Plot 7			
	Tree (%)	Shrub (%)	NPV (%)	Bare (%)	Tree (%)	Shrub (%)	NPV (%)	Bare (%)
ME	-0.3	-3.1	0.5	1.3	-0.3	-3.9	-1.9	4.6
MAE	0.7	4.4	5.4	7.8	0.8	4.3	3.5	5.4
RMSE	1.5	4.8	7.9	10.8	1.6	4.8	3.9	6.0

Abbreviations: ME = mean error, MAE = mean absolute error, RMSE = root mean squared error.

little green foliage being identified as NPV. However, while this is technically accurate, classification as shrub would be most informative for management purposes because bare branches are part of live vegetation.

The estimated fractional cover of surface types has positive linear correlation with the reference cover (Figure 9). The correlation ranged from 0.11 to 0.70 when analyzing all plots and from 0.46 to 0.77 when excluding Plot 7 from analysis. Gentle slopes of trees (0.53–0.54) and shrubs (0.26–0.43) suggested underestimation of green vegetation cover, as recognized in the accuracy statics (Table 6). When excluding Plot 7 from calculation, the corrections for NPV and bare ground considerably improved, from 0.34 to 0.73 for NPV and from 0.11 to 0.77 for bare ground. Improving the differentiation between NPV and bare ground would significantly enhance the indicative power of remote sensing for estimating fractional cover of land cover types.

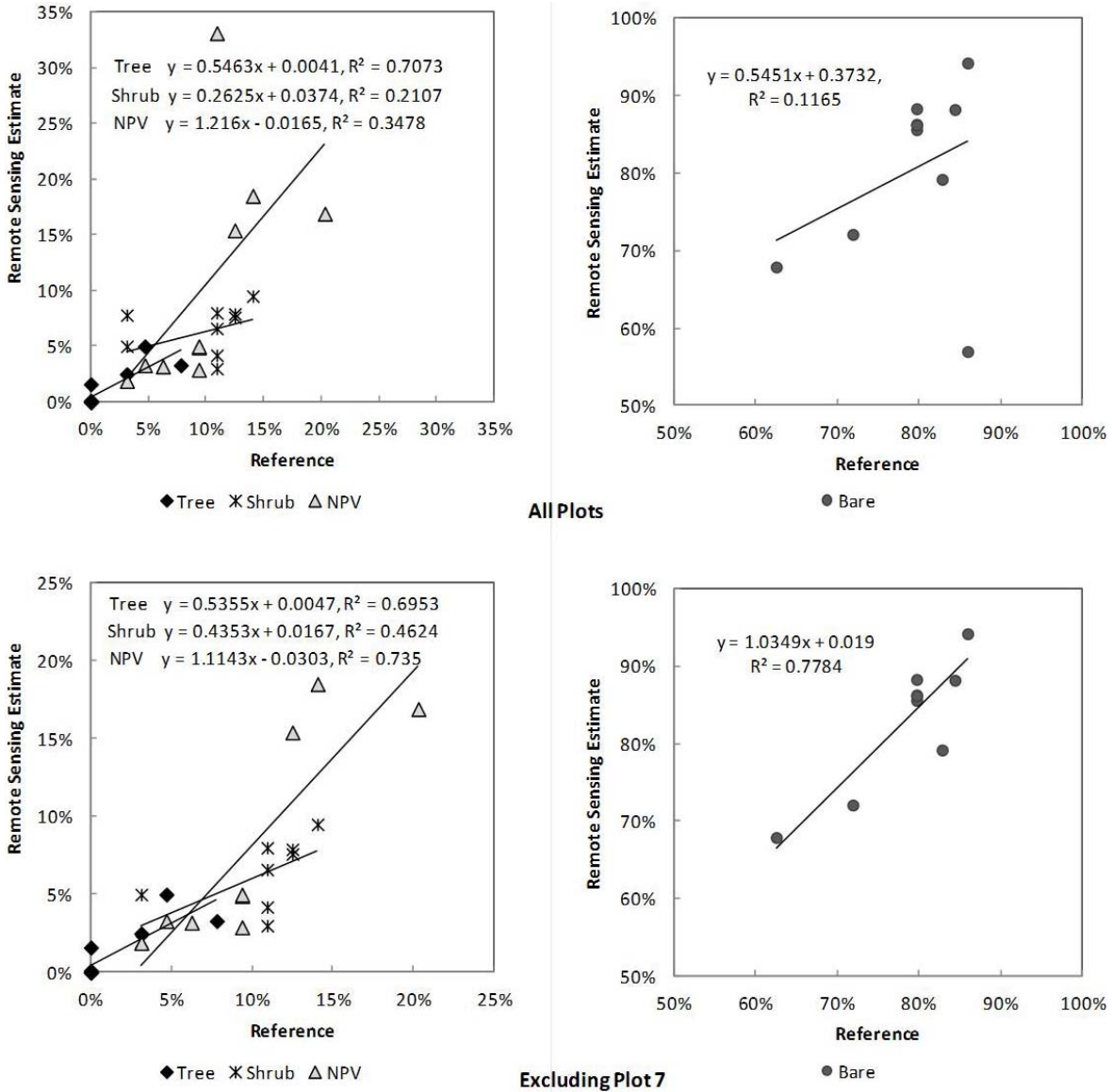


**FIGURE 9 Correlation between Reference Cover and Cover Estimated Using Remote Sensing, Calculated Using All Plots (top) and Excluding Plot 7 (bottom)**

#### 4.2.2 Vegetation Height Estimate

Vegetation height estimated using the image-based point-cloud data was moderately correlated with the vegetation height recorded in the field ( $R^2 = 0.24$ ) (Figure 10). Based on data from the 40 survey points, the following linear function was developed and applied to all survey locations:

$$\text{Vegetation Height (cm)} = \text{PointCloudValue} * 1519 + 13.047, \quad (3)$$

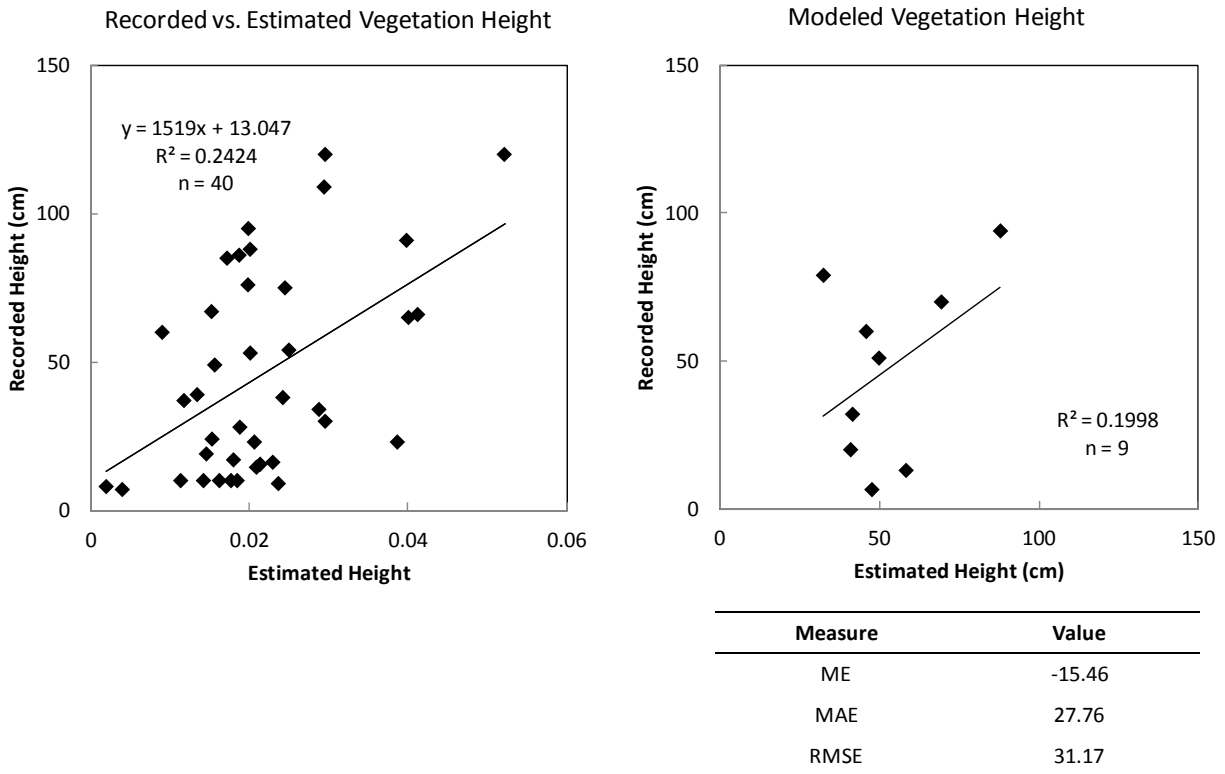


**FIGURE 10 Correlation between Recorded Vegetation Height and Plant Height Estimated Using Remote Sensing (left) and Modeled Vegetation Height with Accuracy Measures (right)**

The correlation between the modeled vegetation height and the recorded vegetation height was weak to moderate ( $R^2 = 0.20$ ) (Figure 10 right). According to the accuracy measures, the model had a negative bias in height estimate ( $ME = -15.46$ ). The average error was approximately 30 cm, and validation samples did not appear to have substantial outliers based on the relatively comparable magnitude of error between MAE and RMSE ( $MAE = 27.76$ ,  $RMSE = 31.17$ ).

The vegetation height map of individual vegetation features is shown in Figure 11. Clusters of trees and tall shrubs that form large vegetation patches along ephemeral channels indicated higher height values than small shrubs (i.e., scrubs) that were shown as small individuals scattered across the area. While the distribution of vegetation height across the area appears spatially cohesive and reasonable, quantitative evaluation of height estimates is warranted in order to substantiate the effectiveness of the approach.

The image-based point-cloud data should ideally indicate the actual height of ground or surface features. That requires highly accurate elevation and height measurement of features using a survey-grade GPS instrument from a large number of survey locations. We attempted to collect survey-grade GPS data during the 2014 field work, but because of unforeseen instrument malfunction during data collection and/or data transfer, we could not retrieve the data despite all possible attempts. Collecting high-density, highly accurate and precise data from ground and

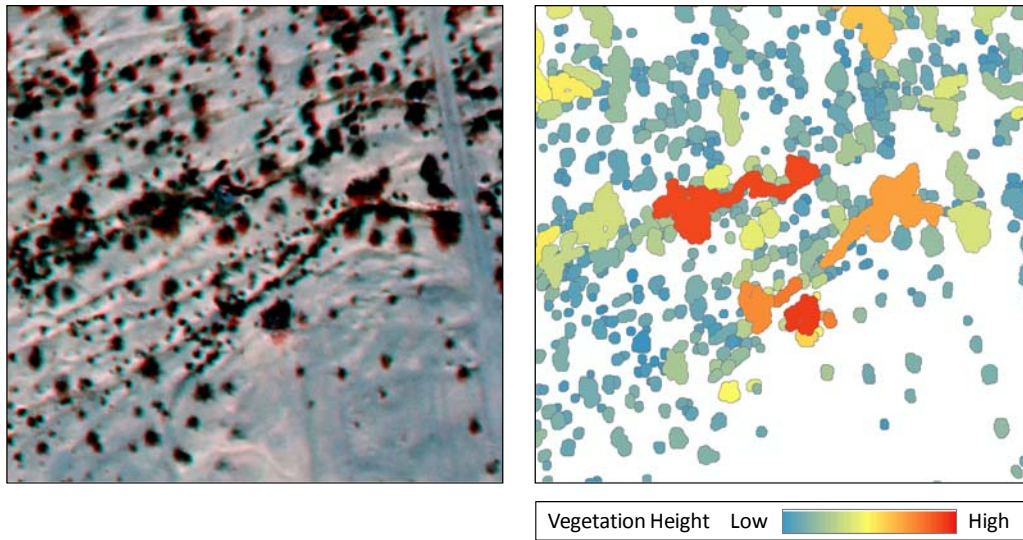


**FIGURE 11 Close-Up Views of Very High Spatial Resolution Image (left)  
Feature-Based Vegetation Height Map Derived from Image-Based Point-Cloud  
Data (right)**

surface features that are invariant over time, in conjunction with identifying a sufficient number of surface features that can be used to generate tie points for height calculation for the aerial triangulation approach, would significantly increase the utility of the image-based point-cloud data for extracting vegetation height.

### **4.3 SOIL AND SURFACE PROPERTIES**

#### **4.3.1 A New Remote Sensing Metric for Assessing Surface Stability, the Erosion Resistance Index**

The ERI maps that were derived from Equation 2 showed spatially cohesive distributions of relatively high and low ERI values across the study area. Figure 12 shows close-up views of output from the 2012 and 2014 images that represent a range of surface types. In Figure 12 (Desert Pavement), intact portions of desert pavement had high index values (warm colors: red, orange, and yellow), while mechanically disturbed surface materials from recreational activities appeared as linear features with lower index values than the intact areas (cool colors: blue and magenta). The range of colors appeared to correspond to the severity of degradation. In Figure 12 (Desert Scrubland), stream beds in a large ephemeral wash, which often contain scattered scrubs in the study area, showed extremely low index values (cool colors). As expected, scrub canopies in Figure 12 (Desert Scrubland), denoted by warm colors, were indicated to have high resistance to erosion.

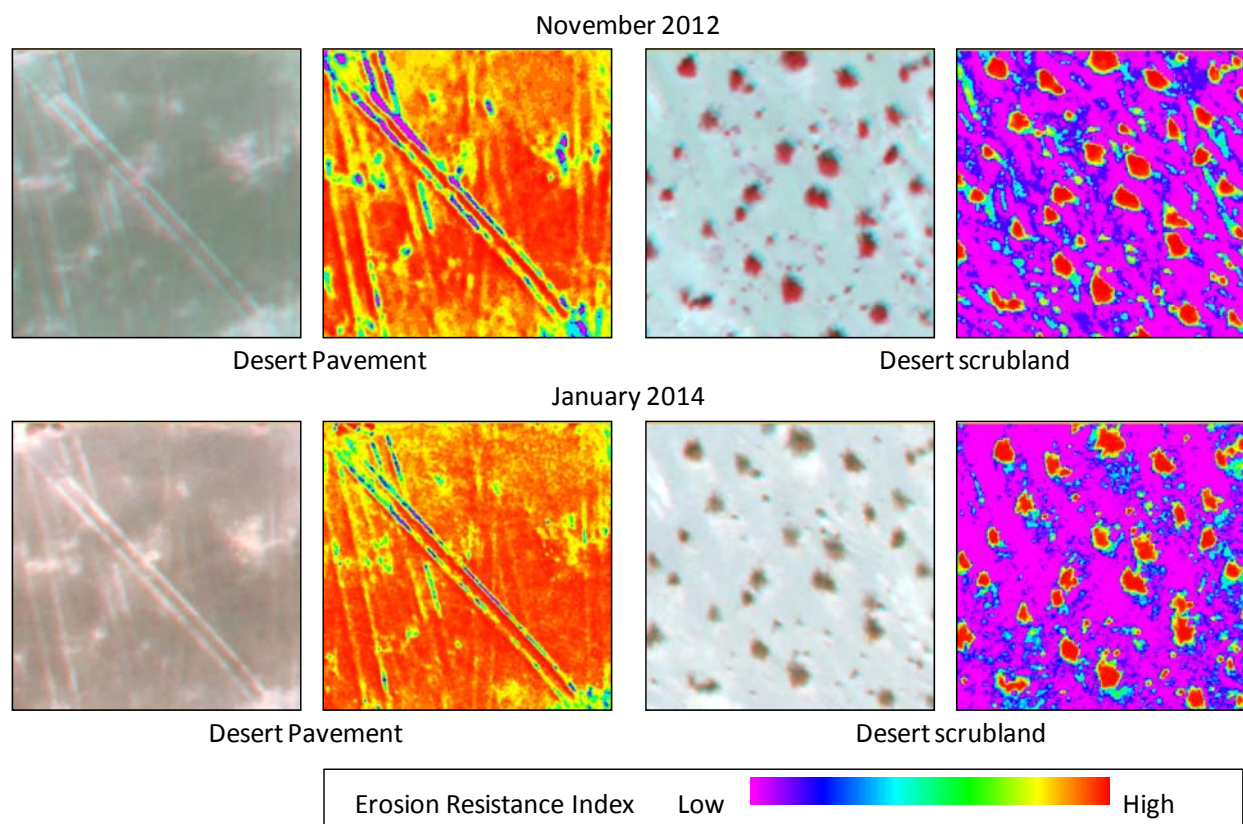


**FIGURE 12 Close-Up View of Surface Stability Index Maps Derived from the Very High Spatial Resolution Image**

Box plots of ERI values from the 2012 and 2014 layers showed a trend of increasing index values from more erodible sandy soil-dominant surface types to more stable rock fragment-dominant surface types, suggesting the index accurately characterized soil stability. However, some differences were apparent between the 2012 and 2014 results. In the 2012 ERI plot, the six surface types can be classified into four groups: surface dominated by loose sandy soil, surface with noticeable nonsoil materials, surface containing substantial rock fragments, and surface completely covered by rock fragments. The first group is represented by stream beds and unpaved roads. The second group contains mixtures of soil, vegetation, and gravels. The third and fourth groups correspond to disturbed and undisturbed desert pavement, respectively. Pairwise t-tests indicated no significant differences in the index values of stream beds and unpaved roads in 2012 (Table 7;  $p = 0.642$ ), while the ERI values for the rest of the surface types were significantly different from each other ( $p < 0.05$ ). In contrast, in 2014, the difference in ERI values between stream beds and unpaved roads was statistically significant ( $p = 0.019$ ; Table 7), despite some overlap in index values. In addition, unpaved roads were indistinguishable from scrubland and bare ground containing substantial amounts of gravels. The two desert pavement surface types showed good separation from each other and the other three surface types in both 2012 and 2014 ( $p < 0.05$ ).

**TABLE 7 Pairwise t-Test Results for the Comparison of the Erosion Resistance Index Values for Five Land Surface Cover Types**

Surface Type	Stream Bed	Unpaved Roads	Scrubland	BG with Gravels	DP (disturbed)
November 2012					
Unpaved roads	0.642	–	–	–	–
Scrubland	4.60E-09	5.60E-09	–	–	–
BG with gravels	8.60E-12	1.10E-13	0.028	–	–
DP (disturbed)	2.00E-16	2.00E-16	2.00E-08	2.30E-06	–
DP (intact)	2.00E-16	2.00E-16	1.30E-12	3.60E-13	3.90E-08
January 2014					
Unpaved roads	0.0019	–	–	–	–
Scrubland	0.0024	0.4706	–	–	–
BG with gravels	4.50E-06	0.1473	0.0012	–	–
DP (disturbed)	1.30E-10	1.30E-07	1.60E-11	6.60E-08	–
DP (intact)	1.20E-15	9.00E-14	2.00E-16	4.80E-16	1.60E-12

Abbreviations: BG = bare ground, DP = desert pavement.

### 4.3.2 Soil Properties and Remote Sensing Metrics

Most combinations of soil properties and remote sensing metrics were significantly correlated, suggesting the remote sensing metrics were powerful indicators of soil properties (Table 8). The equations for each relationship in Table 8 are presented in Table 9. The equations relating the percentage of total carbon and percentage of inorganic carbon to vegetation density were nearly the same for both the 15-cm- and 1.5-m-resolution remote sensing metrics. The similarity was likely due to the fact that total inorganic carbon accounted for nearly two-thirds of all the carbon present in the soil samples. All of the relationships, except one, that are identified in Table 8 come from the lower (5–10 cm) soil sample dataset. One hypothesis to account for this fact is that the first 5 cm of soil is highly variable due to aeolian or other sedimentation processes.

Using the equations in Table 9, one can potentially map soil properties for the whole study area, providing information about the soil over a much larger area than the physical samples alone. However, a significant number of additional soil samples are needed to achieve greater certainty regarding the accuracy of these equations. Despite the uncertainty, these results are exciting and provide a potential new way in which to use remote sensing data. If the additional sampling and analysis indicate that the equations are robust, this analysis could be extended to other desert environments and locations to see if these correlations and relational functions are location and environment specific.

**TABLE 8 Correlation Analysis Results for the Relationships between Remote Sensing Metrics and Soil Properties**

Depth and Resolution	Correlation Relationship <sup>a</sup>	Pearson Corr. Coeff.	Spearman Corr. Coeff.	Linear or Monotonic	P-value
Shallow, 15 cm	pH vs. pc1_tex	0.641	0.684	Linear	0.000
Deep, 15 cm	TotalCarb_Pcnt vs. pc1_tex	-0.681	-0.675	Linear	0.003
	TotalCarb_Pcnt vs. veg_dense	-0.736	<b>-0.953<sup>b</sup></b>	Monotonic	0.000
	TotalOrganCarb_Pcnt vs. pc1_tex	-0.599	-0.675	Monotonic	0.004
	TotalInorganicCarb_Pcnt vs. pc1_tex	-0.600	-0.503	Linear	0.014
	TotalInorganicCarb_Pcnt vs. veg_dense	-0.712	-0.911	Monotonic	0.000
	TotalNitrog_Pcnt vs. pc1_tex	-0.632	-0.710	Linear	0.009
	Sand_Pcnt vs. veg_dense	0.688	0.543	Linear	0.003
	Clay_Pcnt vs. veg_dense	-0.516	-0.644	Monotonic	0.012
Deep, 1.5 m	TotalCarb_Pcnt vs. MSAVI	-0.602	-0.644	Linear	0.013
	TotalCarb_Pcnt vs. pc1_tex	-0.723	-0.770	Linear	0.002
	TotalCarb_Pcnt vs. SSI	-0.620	-0.644	Linear	0.010
	TotalCarb_Pcnt vs. veg_dense	-0.690	-0.810	Monotonic	0.000
	TotalInorganicCarb_Pcnt vs. MSAVI	-0.622	-0.655	Linear	0.010
	TotalInorganicCarb_Pcnt vs. veg_dense	-0.735	-0.894	Monotonic	0.000
	TotalNitrog_Pcnt vs. pc1_tex	-0.717	-0.825	Monotonic	0.000
	TotalNitrog_Pcnt vs. $\rho_{green}$	0.451	0.607	Monotonic	0.013
	TotalNitrog_Pcnt vs. $\rho_{red}$	0.385	0.600	Monotonic	0.014

<sup>a</sup> Abbreviations: pc1 = first principal component, TotalCarb\_Pcnt = % total carbon, veg\_dense = vegetation density, TotalOrganCab\_Pcnt = % total organic carbon, TotalInorganicCarb\_Pcnt = % total inorganic carbon, TotalNitrog\_Pcnt = % total nitrogen, Sand\_Pcnt = % sand, Clay\_Pcnt = % clay, MSAVI = modified soil-adjusted vegetation index,  $\rho_{green}$  = spectral reflectance value of the green band,  $\rho_{red}$  = spectral reflectance value of the red band.

<sup>b</sup> Statistically significant correlations are represented by coefficients in bold.

### 4.3.3 Biological Soil Crust and Remote Sensing Metrics

According to the sample data, the area containing biological soil crust was confined to a small range of the BSCI value (BSCI = 3.09–3.54) (Figure 13). Areas having low BSCI values were often channel beds or areas that were covered with loose sandy soils. Areas having high BSCI values corresponded to vegetation, dark soils, and desert pavement. Extremely large BSCI values (BSCI>5) corresponded to shadows caused by the topographic relief.

Biological soil crusts in the study area were predominantly Cyanobacteria-dominated. Field validation and further examination are warranted for better understanding of the relationship between the occurrence of biological soil crusts and BSCI because of (1) insufficient

**TABLE 9 Equations Describing the Relationship of Remote Sensing Metrics to Soil Properties**

Depth and Resolution	Relationship Function	Significance Level <sup>a</sup>
Shallow, 15 cm	$pH = 8.37 + 3.95 \times pc1\_tex$	*
Deep, 15 cm	$TotalCarb\_Pcnt = (0.684 - 2.337 \times pc1\_tex) \times 100$	*
	$TatalCarb\_Pcnt = (0.494 \times veg\_dens^{-0.021}) \times 100$	**
	$TotalOrganCarb\_Pcnt = (0.102 \times veg\_dens^{-0.092}) \times 100$	***
	$TotalInorganicCarb\_Pcnt = (0.532 - 2.041 \times pc1\_tex) \times 100$	**
	$TotalInorganicCarb\_Pcnt = (0.361 \times veg\_dens^{-0.026}) \times 100$	**
	$TotalNitrog\_Pcnt = (0.017 - 0.062 \times pc1\_tex) \times 100$	*
	$Sand\_Pcnt = (0.794 + 0.135 \times veg\_dens) \times 100$	*
	$Clay\_Pcnt = (0.080 - 0.068 \times veg\_dens) \times 100$	**
Deep, 1.5 m	$TotalCarb\_Pcnt = (0.688 - 1.456 \times MSAVI) \times 100$	**
	$TotalCarb\_Pcnt = (0.718 - 2.800 \times pc1\_tex) \times 100$	*
	$TotalCarb\_Pcnt = (0.648 - 1.334 \times ERI) \times 100$	*
	$TotalCarb\_Pcnt = (0.502 \times veg\_dens^{-0.021}) \times 100$	**
	$TotalInorganicCarb\_Pcnt = (0.514 - 1.195 \times MSAVI) \times 100$	*
	$TotalInorganicCarb\_Pcnt = (0.360 \times veg\_dens^{-0.025}) \times 100$	**
	$TotalNitrog\_Pcnt = (0.004 \times pc1\_tex^{-0.431}) \times 100$	*
	$TotalNitrog\_Pcnt = (0.037 \times \rho_{green}^{0.567}) \times 100$	***
	$TotalNitrog\_Pcnt = (0.028 \times \rho_{red}^{0.481}) \times 100$	n.s.

<sup>a</sup> \* = Coefficients and exponents are significant at  $\alpha = 0.01$ ; \*\* = coefficients and exponents are significant at  $\alpha = 0.05$ ; \*\*\* = coefficients and exponents are significant at  $\alpha = 0.1$ ; n.s. = coefficients and exponents not significant at  $\alpha = 0.1$ .

field survey data, (2) potential incompatibility in spatial scale between BSCI and input images, (3) type of biological soil crusts (moss and lichen versus cyanobacteria), (4) extremely sparse and discontinuous distribution of biological soil crusts in the study area, and (5) incompatibility in band positioning between Landsat and the VHSR images.

#### 4.4 EFFECTIVE REMOTE SENSING METRICS FOR EXTRACTING AND CHARACTERIZING DESERT LANDSCAPE FEATURES AND PROPERTIES

Several remote sensing metrics were identified to be effective for extracting and characterizing landscape features and properties that were important for long-term environmental monitoring in desert regions (Table 10). Spectral reflectance values of the green, red, and NIR spectral regions were found to be essential for obtaining information about desert landscapes. Of all the SVIs tested, VARI was the most useful for detecting desert vegetation with small canopy

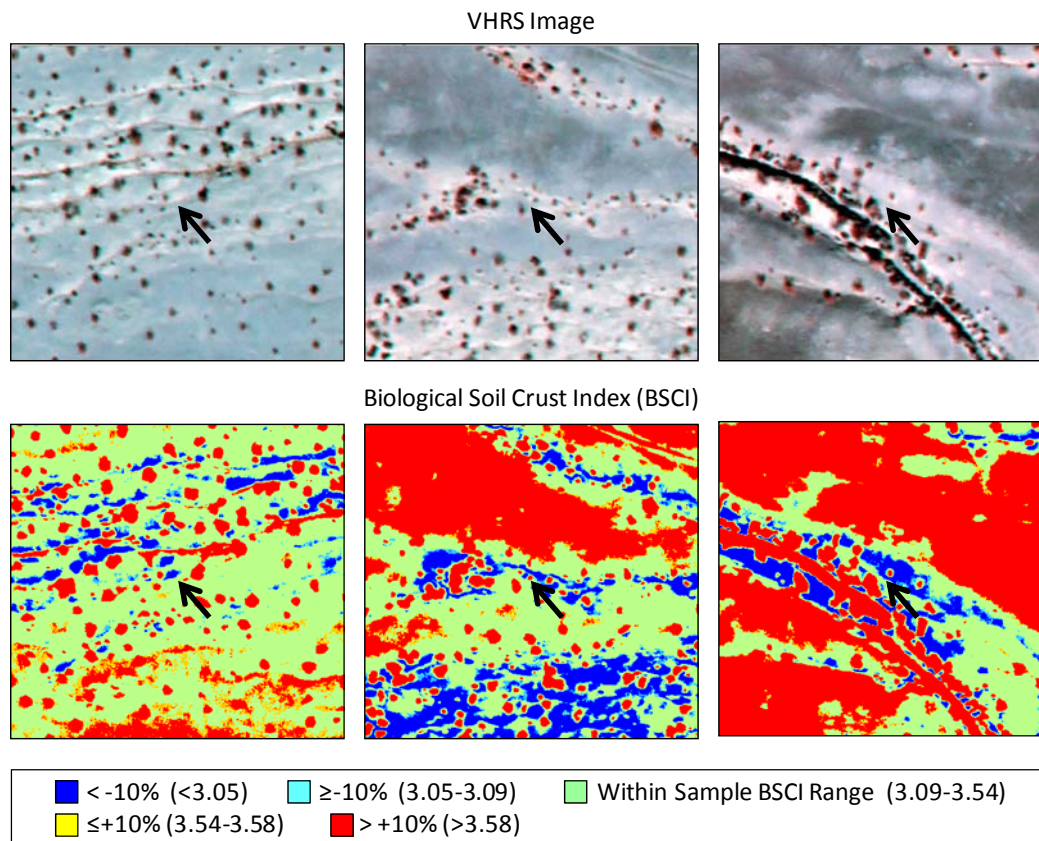


**FIGURE 13 Close-Up Views of Biological Soil Crust Index Maps Derived from the Very High Spatial Resolution Image**

**TABLE 10 Monitoring Indicators Tested and Remote Sensing Metrics Identified in This Study**

BLM Core Indicators Tested in This Study	Supplemental Indicators Tested in This Study	Remote Sensing Metrics
Vegetation <ul style="list-style-type: none"> <li>• Amount of bare ground cover</li> <li>• Vegetation composition</li> <li>• Vegetation height</li> </ul>	<ul style="list-style-type: none"> <li>• Photosynthesis</li> </ul>	Visible atmospherically resistant index (VARI)  Spectral reflectance values Digital surface model (DSM) Digital terrain model (DTM)
Soil (or surface) <ul style="list-style-type: none"> <li>• Soil aggregate stability</li> </ul>	<ul style="list-style-type: none"> <li>• Particle size distribution</li> <li>• Soil moisture</li> <li>• Soil organic carbon</li> </ul>	Erosion resistance index (ERI) First principal components (PC1) Spectral reflectance values

size with sparse foliage cover. Its robustness to environmental variability makes VARI a very desirable metric for long-term monitoring using time-series remotely sensed datasets. Relative height information obtained from the image-based DSM and DTM provided useful information for differentiating trees (mostly consisting of microphyll tree species) and shrubs (creosotebush and white bursage), each of which have different functions in ecosystems. Precise spatial fidelity between spectral and height information achieved by deriving information from a common dataset would be extremely beneficial for fine-scale landscape characterization, which is problematic when using LiDAR data. Improving the accuracy of DTM will further increase the accuracy of canopy height measurement.

Overall brightness was the primary characteristic used to understand the distribution and categories of surface in desert landscape. The output from the principal component analysis is dependent on the spectral variation of the input data, which may affect the repeatability of the algorithm because environmental conditions (e.g., sun angle and cloud cover) influence incident and reflected energy level. However, the principal component analysis is considered useful because spectral characteristics within the study area are expected to be relatively stable or often remain unchanged.

Directly linking remote sensing metrics to monitoring indicators was quite challenging because of the lack of typical soil aggregate needed for calibration and validation and the limited exposed soil in the study area. A new remote sensing metric, ERI, was developed to quantify the resistance of soil and non-soil surface to erosion. Although the robustness of the index is warranted, ERI indicated its ability to examine bare ground in dry land comprehensively.

*This page intentionally left blank.*

## 5 CONCLUSIONS AND FUTURE WORK

Argonne developed scientifically valid, cost-effective remote sensing methodologies for characterizing landscape features and properties, and identified remote sensing metrics to support BLM's development of financially sustainable long-term environmental monitoring strategies for desert regions where multiple utility-scale solar developments are anticipated. The effectiveness of remote sensing technologies, particularly VHSR imagery, was examined for three land resource categories: surface hydrologic features, vegetation, and soil (or surface). For vegetation and soil, the study directly or indirectly examined eight monitoring indicators—amount of bare ground, vegetation composition, vegetation height, photosynthesis, soil stability, soil moisture, soil organic carbon, and particle distribution. Our results indicate that the monitoring method accurately characterized the fractional cover of tree, shrub, NPV, bare ground, and soil stability, all of which are core indicators used for the long-term monitoring plan for BLM's Riverside East SEZ.

Argonne developed an algorithm capable of extracting a range of channel types to generate detailed distributions of ephemeral stream networks in greater detail than the commonly utilized USGS NHD. The algorithm detected 900% more ephemeral streams than were mapped in the study area in the NHD. While well-defined channels were detected with high accuracy, channels having a weak association with dense vegetation growth had varying detection success. In conjunction with spatial filtering operation, PC1 and an SVI (MSAVI was used in the prototype development) were determined as useful remote sensing metrics during the algorithm development. Despite the modest accuracy of the quantitative assessment, the high recognition rate from the qualitative assessment suggests spatial cohesiveness of extracted ephemeral channel segments and their strong association with ephemeral channels present in the study area. This result indicates that inclusion of a pattern recognition routine to the algorithm could further improve channel extraction accuracy, as well as effectiveness of the current algorithm.

The ephemeral channel extraction algorithm also generates intermediate products (e.g., vegetation greenness and vegetation density) that could be useful for understanding other resource types. While the detailed mapping of ephemeral stream networks is a necessary first step, the value of these data to land managers would be enhanced by identifying remote sensing metrics that indicated whether the channels were hydrologically active or inactive.

A combination of spectral reflectance values, VARI, and height information derived from the VHSR multispectral imagery was capable of accurately differentiating two vegetation types—trees, which primarily consisted of microphyll species, and shrubs mostly creosotebush and white bursage—and two bare ground types—mixed surface and desert pavement—in desert landscapes. NPV and bright or light-colored soil that consisted of silt and sand were a source of confusion due to their spectral similarity and intricate combinations across the landscape. One possible solution to this problem would be to collect images shortly after a rain event so that herbaceous plants are green and separable from soil. However, distinguishing dry plant litter from soil would likely remain a challenge.

Height information obtained from the image-based DTM and DSM was particularly effective for differentiating between trees and shrubs, which have similar spectral responses in dry lands. Although two soil types and desert pavement were merged into a single bare ground class in this study, these surface types can be treated independently. In particular, mapping desert pavement would be useful for assessing surface disturbance and degradation from recreational activities or natural causes. During the analysis, VARI that was not necessarily formulated to account for impacts from bright soil background yielded the highest accuracy among 10 SVIs examined. VARI also showed potential robustness to environmental variability in desert regions because the difference of threshold values between two datasets was only 1% of its possible range (from -1 to 1). The SVI used in the ephemeral channel extraction algorithm, MSAVI, will be replaced with VARI in future analysis in order to improve the accuracy of extraction.

The function that was developed from the image-based point-cloud data showed weak to moderate correlation with the recorded vegetation height in the field. Error in vegetation height estimate was approximately 30 cm and generally underestimated. The aerial triangulation technique should ideally yield the actual height of ground or surface features to be most useful. To accomplish the goal, collecting high-density, highly accurate and precise data from ground and surface features that are invariant over time, in conjunction with a sufficient number of identifiable surface features, would significantly increase the utility of the image-based point-cloud data for estimating vegetation height.

Various exploratory analyses were performed to examine the effectiveness of remote sensing for the monitoring metrics of potential use in the Riverside East LTMP—the development of a new remote sensing metric for surface stability, the development of functions for soil properties, and the examination of BSCI. In addition, a remote sensing metric, the ERI, was developed by analyzing ratios of spectral reflectance values extracted from a range of surface types having varying surface stability. Index values were generally greater for the surface types that were expected to be more stable (e.g., desert pavement) and lower for those surface types that are likely unstable (e.g., stream beds and unpaved roads). Confusion between surface types observed in output from both 2012 and 2014 data could largely be explained by the arbitrary nature of surface type definition. Identifying a parameter for surface stability is needed to directly link ERI to erosion risks and evaluate true predictive power of the index. Although the ERI needs further refinement, it shows promise as a tool for mapping surface stability and erosion risks. By mapping susceptibility to surface stability change, the ERI can be used to determine solar development avoidance areas and to identify monitoring priority areas based on their high risk of erosion. In addition, the ERI can be used to monitor future solar energy related surface change and disturbance. For example, a significant change in the index value could indicate the shift of land cover from one state to another (e.g., from desert pavement to exposed soil), which may be linked to increased erosion from solar construction activities.

The BSCI indicated that the area containing sparsely distributed biological soil crust was found within a small range of the BSCI value (BSCI = 3.09–3.54). Further field validation and examination are warranted to draw conclusive outcomes for the relationship between presence of biological soil crusts and BSCI for several reasons, including (1) insufficient field survey data, (2) potential incompatibility in spatial scale between BSCI and input images, (3) type of biological soil crusts (moss and lichen versus cyanobacteria), (4) extremely sparse and

discontinuous distribution of biological soil crusts in the study area, and (5) incompatibility in band positioning between Landsat and the VHSR images.

This study revealed that a few common remote sensing metrics are useful for more than one resource type, and that output from a method for one resource type can serve as input for another resource type. For example, the output layer that indicated that a photosynthetic rate was, in fact, the input for mapping vegetation distribution, and the vegetation map was then used as input for mapping vegetation composition (or fractional cover of surface types) and identifying distribution and abundance of riparian corridors for extracting ephemeral stream channels. This linkage suggests that it is possible to integrate independent image processing algorithms and methods into a single tractable workflow to optimize the efficiency of information extraction. If so, a single VHSR image set could serve as a common data source to produce numerous types of information cost effectively. In addition to the monitoring indicators examined in this study, the output from the remote sensing methodologies can be used to study other resource types. For example, remote sensing metrics that characterize vegetation density provide a basis for understanding the distribution and conditions of critical wildlife habitat. Thus, the remote sensing methodologies developed in this study can potentially be applied to monitoring a broad range of plant and animal resources.

The remote sensing algorithms developed in this study were applicable to multiple resources that will be monitored under the Riverside East LTMP. Although the resource characterization algorithms described in this report show great promise for long-term monitoring applications, additional work is needed before integrating these remote sensing methodologies into BLM's long-term monitoring framework and/or the monitoring plan required for an existing or planned utility-scale solar energy development. For example, because of changes in environmental conditions (e.g., sun angle and cloud cover) between image collection dates, it is essential to test the robustness of remote sensing algorithms across images from multiple dates. Therefore, to facilitate operational use of the remote sensing methodologies developed in this study, examining their applicability for multi-date remotely sensed imagery is essential. The examination should include determining (1) types and magnitude of environmental changes that can be detected and quantified using the methodologies; (2) robustness and sensitivity of the methodologies for anticipated natural environmental variability across a time series of remotely sensed images; and (3) required types and levels of image data preparation for automated, systematic analysis to produce consistent output. In addition to providing a cost-effective monitoring approach, the methods developed in this study can ultimately reduce soft-costs for developers by accurately characterizing the ecological resources at a potential development site, which would potentially reduce permitting and mitigation costs and speed up the siting process.

*This page intentionally left blank.*

## 6 REFERENCES

- BLM (U.S. Bureau of Land Management), 2012, *Approved Resource Management Plan Amendments/Record of Decision (ROD) for Solar Energy Development in Six Southwestern States*, Oct.
- BLM and DOE (BLM and U.S. Department of Energy), 2012, *Final Programmatic Environmental Impact Statement (PEIS) for Solar Energy Development in Six Southwestern States*, FES 12-24, DOE/EIS-0403, Washington, DC, July.
- Chen J., et al., 2005, “A New Index for Mapping Lichen-dominated Biological Soil Crusts in Desert Areas,” *Remote Sensing of Environment* 96:165–175.
- Duncan, J., et al., 1993, “Assessing the Relationship between Spectral Vegetation Indices and Shrub Cover in the Jornada Basin, New Mexico,” *International Journal of Remote Sensing* 14:3395–3416.
- Friedl, M.A., K.C. McGwire, and D.K. McIver, 2001, “An Overview of Uncertainty in Optical Remotely Sensed Data for Ecological Applications,” in *Spatial Uncertainty in Ecology*. G.T. Hunsaker, et al. (editors), Springer, NY.
- Gitelson, A.A., et al., 2002, “Novel Algorithms for Remote Estimation of Vegetation Fraction,” *Remote Sensing of Environment* 1:76-78.
- Hamada, Y., D.A. Stow, and J. Franklin, 2010, “Quantifying Biological Integrity of California Sage Scrub Communities Using Plant Life-form Cover,” *Journal of Mediterranean Ecology* 10:19–32.
- Hamada, Y., et al., 2013, “Assessing and Monitoring Semi-arid Shrublands Using Object-based Image Analysis and Multiple End Member Spectral Mixture Analysis,” *Environmental Monitoring and Assessment* 184(4):3173–3190.
- Hamada, Y., D.A. Stow, and D.A. Roberts, 2011, “Estimating Life-form Cover Fractions within California Sage Scrub Communities Using Remote Sensing,” *Remote Sensing of Environment* 115(12):3056–3068.
- Herrick, J.E., et al., 2005, *Monitoring Manual for Grassland, Shrubland and Savanna Ecosystems*, USDA-ARS Jornada Experimental Range.
- Huete, A.R., 1988, “A Soil-adjusted Vegetation Index (SAVI),” *Remote Sensing of Environment* 25:295–309.
- Huete, A., et al., 2002, “Overview of the Radiometric and Biophysical Performance of the MODIS Vegetation Indices,” *Remote Sensing of Environment* 83:195–213.

Jensen, J.R., 2000, *Remote Sensing of the Environment: An Earth Resource Perspective*, Prentice Hall, NJ.

Jiang, Z., et al., 1998, "Development of a Two-band Enhanced Vegetation Index without a Blue Band," *Remote Sensing of Environment* 112(10):3833–3845.

Karnieli, A., et al., 1997, "Spectral Characteristics of Cyanobacteria Soil Crust in Semiarid Environments," *Remote Sensing of Environment* 69:67–75.

Nagy, M.L., A. Pérez and F. Garcia-Pichel. 2005. The prokaryotic diversity of biological soil crusts in the Sonoran Desert (Organ Pipe Cactus National Monument, AZ). *FEMS Microbiology Ecology* 54:233–245.

Okin, G.S., et al., 2001, "Practical Limits on Hyperspectral Vegetation Discrimination in Arid and Semiarid Environments," *Remote Sensing of Environment* 77:212–225.

Perry, C.R., and L.F. Lautenschlager, 1984, "Functional Equivalence of Spectral Vegetation Indices," *Remote Sensing of Environment* 14(1-3):169–182.

Qi, J., et al., 1994, "Modified Soil Adjusted Vegetation Index (MSAVI)," *Remote Sensing of Environment* 48(2):119-126. doi:10.1016/0034-4257(94)90134-1.

Rondeaux, G., and F. Baret, 1996, "Optimization of Soil-induced Vegetation Indices," *Remote Sensing of Environment* 55:95–107.

Stow, D., 1995, "Monitoring Ecosystem Response to Global Change: Multitemporal Remote Sensing Analyses," in *Global Change and Mediterranean-Type Ecosystems*, J.M. Moreno and W.C. Oechel (editors), Springer, NY.

Taylor, J.J., et al., 2014. *AIM-Monitoring: A Component of the BLM Assessment, Inventory, and Monitoring Strategy*, Technical Note 445, U.S. Department of the Interior, Bureau of Land Management, National Operations Center, Denver, CO.

Toevs, G.R., et al., 2011, Bureau of Land Management Assessment, Inventory, and Monitoring Strategy: For Integrated Renewable Resources Management, Bureau of Land Management, National Operations Center, Denver, CO.

Tou, J.T., and R.C. Gonzalez, 1974, *Pattern Recognition Principles*, Addison-Wesley Publishing Company.

Tucker, C.J., 1979, "Red and Photographic Infrared Linear Combinations for Monitoring Vegetation," *Remote Sensing of Environment* 8:127–150.

USGS (U.S. Geological Survey), 2008, *National Hydrography Dataset*. Available at <http://nhd.usgs.gov>.





## **Environmental Science Division**

Argonne National Laboratory  
9700 South Cass Avenue, Bldg. 240  
Argonne, IL 60439-4847

[www.anl.gov](http://www.anl.gov)



Argonne National Laboratory is a U.S. Department of Energy  
laboratory managed by UChicago Argonne, LLC